Bulletin of Engineering Geology and the Environment (2020) 79:4167–4190
https://doi.org/10.1007/s10064-020-01798-8

ORIGINAL PAPER

# Design equation for stability of shallow unlined circular tunnels in Hoek-Brown rock masses

Suraparb Keawsawasvong [1] · Boonchai Ukritchon [2,3]

Received: 23 August 2019 / Accepted: 8 April 2020 / Published online: 29 April 2020


## Abstract
Safety assessment is one critical issue for constructions of tunnels and requires a reliable and accurate stability analysis. At present, a large number of researches in stability analyses of tunneling in rock masses have been conducted; however, a lack of an accurate and reliable design equation for the tunnel stability prediction is obvious. This paper presents a new design equation for stability analyses of shallow unlined circular tunnels in rock masses obeying the Generalized Hoek-Brown failure criterion. Because of the complexity of the problem's nature, a closed-formed analytical solution of the problem is not possible to be achieved. Hence, the computational framework of the finite element limit analysis is selected to numerically derive the upper and lower bound solutions of the problem. A complete set of the dimensionless parameters covering the shallow cover-depth ratios of tunnels, the normalized uniaxial compressive strength of intact rocks, and the Hoek-Brown material parameters are comprehensively investigated. A new design equation for stability analyses of shallow unlined circular tunnels in rock masses is developed by employing a nonlinear regression analysis to the numerically derived average bound solutions. It is found that the proposed new design equation is highly accurate and provides a convenient and reliable tool for stability analyses of shallow unlined tunnels in rock masses in practice.

**Keywords** Circular tunnels · Rock mass · Hoek-Brown · Finite element limit analysis · Design equation

**List of notations**

| | |
|---|---|
| $\sigma_1$ | the effective major principal stress |
| $\sigma_3$ | the effective minor principal stress |
| $\sigma_{ci}$ | the uniaxial compressive strength of intact rocks |
| $GSI$ | the Geological Strength Index of rocks |
| $m_i$ | the frictional strength of intact rocks |
| $DF$ | the disturbance factor reflected by blast damage and stress relaxation |
| $D$ | the diameter of circular tunnels |
| $C$ | the cover depth of circular tunnels |
| $\gamma$ | the constant unit weight of rocks |
| $\sigma_s$ | a uniform surcharge applied over the top rock surface |
| $\sigma_s/\sigma_{ci}$ | the normalized collapse surcharge |
| $\sigma_{ci}/\gamma D$ | the normalized uniaxial compressive strength |
| $C/D$ | the cover depth ratio of circular tunnels |
| $q$ | the constant vertical pressure applied on the top plane of plane strain biaxial compression |
| $Q$ | the total vertical compressive load applied to the footing |
| $N$ | the bearing capacity factor |
| $B$ | the full width of footing |
| $A_i$, $B_i$, $E_i$, $G_i$ | initial coefficients for design equation |
| $a_i$, $b_i$, $c_i$, $d_i$, $e_i$, $f_i$, $g_i$ | optimal constant coefficients for design equation |
| $y_i$ | average computed bound solution of $\sigma_s/\sigma_{ci}$ |
| $f_i$ | approximate solution of $\sigma_s/\sigma_{ci}$ |
| $n$ | number of data |

✉ Boonchai Ukritchon
boonchai.uk@gmail.com

Suraparb Keawsawasvong
suraparb@hotmail.com

[1] Department of Civil Engineering, Thammasat School of Engineering, Thammasat University, Pathumthani 12120, Thailand

[2] Centre of Excellence in Geotechnical and Geoenvironmental Engineering, Department of Civil Engineering, Faculty of Engineering, Chulalongkorn University, Bangkok 10330, Thailand

[3] Center of Excellence on Earthquake Engineering and Vibration, Department of Civil Engineering, Faculty of Engineering, Chulalongkorn University, Bangkok 10330, Thailand

$R^2$ the coefficient of determination
$N_c$ the factor representing the effect of the uniaxial compressive strength $\sigma_{ci}$ of intact rocks
$N_\gamma$ the factor representing the effect of rock unit weight $\gamma$

## Introduction

At present, the population growth in an urban area occurs considerably, and hence, the constructions of public infrastructures and utilities have increased accordingly in order to cope with the needs of public transportations to such rapid expansion, especially the constructions of underground structures such as tunnels and subways. Tunnel safety is one very crucial issue for tunnel excavations by an open-face conventional tunneling and/or a tunneling boring machine. Therefore, it is important to assess the stability of tunnels in order to prevent potential catastrophes during tunneling and to reduce the impact of movements induced by tunneling on existing structures. In this paper, the present study of the problem is scoped with the stability analysis of shallow unlined circular tunnels in rock masses.

In addition to laboratory and centrifuge tests on tunnels (Kimura and Mair 1981; Chambon and Corté 1994; Kirsch 2010), the limit analysis (Chen and Liu 1990) is another methodology that can be employed to study the stability of tunnels using an analytical approach (Davis et al. 1980) or a numerical-based finite element and mathematical optimization known as finite element limit analysis (FELA) (Sloan 2013). The FELA technique has been conventionally employed to investigate the stability of single tunnels in soils by many researchers such as plane strain heading of tunnels (e.g., Sloan and Assadi 1994; Augarde et al. 2003; Yang et al. 2016), unlined circular tunnels (e.g., Wilson et al. 2011; Yamamoto et al. 2011a), unlined square tunnels (e.g., Assadi and Sloan 1991; Sloan and Assadi 1991; Wilson et al. 2013; Yamamoto et al. 2011b; Ukritchon and Keawsawasvong 2018a), and stability of retained soils with opening in underground walls (e.g., Ukritchon and Keawsawasvong 2017a, 2019a). Note that those works were performed on soils obeying on the Mohr-Coulomb failure criterion. Since the failure of rock masses cannot be accurately modelled the by Mohr-Coulomb failure criterion owing to the lack of the dependency of rock strength on the nonlinear minor principal (compressive) stress, those existing solutions do not provide an accurate solution for the stability of tunnels in rock masses.

The Hoek-Brown (HB) failure criterion (Hoek et al. 2002) is generally accepted as a better model for estimating the strength of rock masses, as compared with the Mohr-Coulomb failure criterion. The model of the HB failure criterion can capture essential failure aspects of many rock types particularly for the dependency of shear strength of rock masses on the nonlinearity of the minor principal (compressive) stress. As a result, the HB failure criterion has been widely used as the failure law of various stability problems in the field of rock engineering. For example, the studies on bearing capacity and shaft resistance of foundations resting or embedded in rock masses were reported by Serrano and Olalla (1998a, 1998b), Merifield et al. (2006), Clausen (2013), Serrano et al. (2014, 2015, 2016), Chakraborty and Kumar (2015), Keshavarz et al. (2016), Keshavarz and Kumar (2018), Kumar and Mohapatra (2017), and Ukritchon and Keawsawasvong (2018b). In addition, many problems related to underground openings, tunnels, and plane strain headings have been solved using the HB failure criterion such as Carranza-Torres and Fairhurst (1999), Carranza-Torres (2004), Fraldi and Guarracino (2009), Senent et al. (2013), Yang and Huang (2011, 2013), and Ukritchon and Keawsawasvong (2019b, 2019c). The stability analyses of rock slopes with the implementation of the HB failure criterion are also investigated by Akin (2013), Deng et al. (2016), Li et al. (2008, 2011), Shen et al. (2013), Yang et al. (2004), and Belghali et al. (2017).

Regarding the abovementioned works, the solutions of Carranza-Torres and Fairhurst (1999) and Carranza-Torres (2004) are only applicable to very deep circular tunnels under hydrostatic pressures while those of Fraldi and Guarracino (2009) and Yang and Huang (2011, 2013) correspond to the collapse of supported cavity roof of tunnels, which does not consider the collapse of the entire circular shape of tunnels. The work of Senent et al. (2013) is related to the stability analysis of front face of circular tunnels with fully rigid supports while those of Ukritchon and Keawsawasvong (2019b, 2019c) pertain to stability analyses of square tunnels and plane strain heading in rock masses, respectively. Obviously, there is a lack of studies on the stability of shallow unlined circular tunnels in rock masses. The results of the present study are useful in practice since the circular tunnel is a commonly used shape in a practical underground excavation. In particular, there is no design equation currently available in the literature for a stability assessment of shallow unlined circular tunnels in rock masses. Such design equation is desirable and valuable for practicing engineers for performing the stability prediction of underground excavations of circular tunnels in practice.

The aim of this paper is to develop and propose a design equation for shallow unlined circular tunnels in rock masses based on a parametric study using finite element limit analysis (FELA) in which rock masses are modelled by the Hoek-Brown (HB) failure criterion. Both upper bound (UB) and lower bound (LB) FELA calculations are performed to bracket the exact stability solution of shallow unlined circular tunnels in HB materials while the influences of the tunnel cover-depth ratios, the normalized uniaxial compressive strength of intact rocks, and the HB material parameters (i.e., Geological

Strength Index ($GSI$), and the $m_i$ parameter) are comprehensively investigated. The failure mechanisms of circular tunnels are also presented to portray the effects of HB parameters on the stability of circular tunnels in rock masses. Based on a nonlinear regression analysis, a closed-form approximate design equation is developed for stability analyses of shallow unlined circular tunnels in rock masses. The proposed design equation is useful for practicing engineers to conveniently and accurately assess the stability of tunnel excavations by an open-face conventional tunneling and a tunneling boring machine.

## Problem definition and method of analysis

The present study adopts the failure of rock masses governed by the Generalized Hoek-Brown (GHB) failure criterion (Hoek et al. 2002), which are subsequently improved from the original version proposed by Hoek and Brown (1980). The historical review of the development of the GHB model is summarized in Hoek (2004, 2007). The GHB model was developed and updated using a large number of laboratory triaxial tests including field tests of rocks while the effects of highly fractured rocks were also incorporated into the model. The GHB failure criterion controls the strength of rock masses through a power law relationship between the major and minor principal stresses as:

$$-\sigma_3 = -\sigma_1 + \sigma_{ci}\left(-m_b\frac{\sigma_1}{\sigma_{ci}} + s\right)^a \tag{1}$$

where $\sigma_1$ and $\sigma_3$ are the effective major and minor principal stresses (i.e., $\sigma_1 > \sigma_3$), respectively, in which the tension positive sign convention is adopted. $\sigma_{ci}$ is the uniaxial compressive strength of intact rocks. The $GSI$ of a rock mass is used to control the material parameters $m_b$, $s$, and $a$ through the following empirical relationships (Hoek 2004, 2007):

$$m_b = m_i \exp\left(\frac{GSI-100}{28-14DF}\right) \tag{2}$$

$$s = \exp\left(\frac{GSI-100}{9-3DF}\right) \tag{3}$$

$$a = \frac{1}{2} + \frac{1}{6}\left(e^{-\frac{GSI}{15}} - e^{-\frac{20}{3}}\right) \tag{4}$$

$GSI$ is the most important parameter of the Hoek-Brown failure criterion (Hoek et al. 2002) describing the quality of an in-situ rock mass influenced by its structural discontinuities and surface weathering conditions that give rise to $GSI$ in the range of 10–100. The cases of extremely poor rock masses and intact rocks correspond to $GSI = 10$ and 100, respectively. The $DF$ parameter is the disturbance factor that reflects the degree of disturbance to which the rock mass has been subjected by blast damage and stress relaxation. The typical range of $DF$ is 0–1 in which undisturbed in-situ rock masses have $DF = 0$ and extremely disturbed in-situ ones have $DF = 1$. The frictional strength of the intact rock mass is reflected by the $m_i$ parameter while $m_b$ is the reduced parameter of $m_i$ by a factor of an exponential function accounting for an effect of strength reduction of the rock mass conditions defined by $GSI$ and $DF$. Thus, the GHB failure criterion generally requires four input parameters, namely $\sigma_{ci}$, $GSI$, $DF$, and $m_i$, in order to control the strength of in-situ rock masses.

The problem definition of the present study is shown in Fig. 1 corresponding to an infinitely long shallow unlined circular tunnel. The circular tunnel with a diameter ($D$) is located with a cover depth ($C$) in a rock mass obeying the GHB failure criterion. In this study, it is assumed that the method of tunneling excavation does not introduce any significant disturbance to the rock mass, and hence, the disturbance factor $DF$ is set to be zero. Thus, the rock mass obeying the GHB failure criterion has a set of strength parameters of $\sigma_{ci}$, $GSI$, and $m_i$, and a constant unit weight of $\gamma$. A uniform surcharge ($\sigma_s$) is applied over the top rock surface. The surcharge ($\sigma_s$) and the constant unit weight of rock ($\gamma$) result in the active failure of rock masses around the circular tunnel while this failure is resisted by the shear resistance of rock masses attributed from $\sigma_{ci}$, $GSI$, and $m_i$. Thus, the stability analysis of the problem is to determine the collapse surcharge ($\sigma_s$) causing the active failure of tunnels. In this study, it can be shown by the dimensionless technique (Butterfield 1999) that the normalized collapse surcharge of shallow unlined circular tunnels in rock masses under the active failure can be represented by a set of four dimensionless variables as:

$$\frac{\sigma_s}{\sigma_{ci}} = f\left(\frac{C}{D}, \frac{\sigma_{ci}}{\gamma D}, m_i, GSI\right) \tag{5}$$

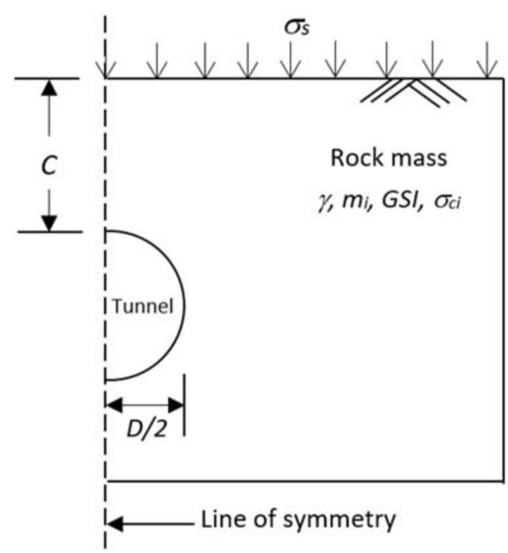


**Fig. 1** Problem definition of infinitely long shallow unlined circular tunnels in rock masses under plane strain condition

where $\sigma_s/\sigma_{ci}$ is the normalized collapse surcharge, $\sigma_{ci}/\gamma D$ is the normalized uniaxial compressive strength, and $C/D$ is the cover-depth ratio of circular tunnels. Note that the $m_i$ and $GSI$ parameters are dimensionless by nature.

In the present study, the upper bound (UB) and lower bound (LB) methods of finite element limit analysis (FELA) under plane strain conditions with the model and computation developed through the computer program OptumG2 (Krabbenhoft et al. 2015) are employed to compute the active collapse of shallow unlined circular tunnels in rock masses. The FELA has become a powerful and efficient tool that is routinely employed to solve a variety of stability problems in geotechnical and rock engineering by the recent authors' works (e.g., Ukritchon and Keawsawasvong 2018b, 2019b, 2019c). This computational limit analysis is based on a perfectly plastic material with an associated flow rule, and employs the plastic bound theorems (Drucker et al. 1952), finite element discretization, and mathematical optimization in order to solve the UB and LB solutions of stability problems by bracketing the true limit load from above and below. The mathematical optimization employed in the method enables it to be powerful and efficient as compared with manual calculations of limit analysis. It should be noted that the UB and LB FELA using OptumG2 have been successfully employed to investigate various stability problems by the authors such as Keawsawasvong and Ukritchon, 2016a, b, 2017a, b, c, d, e, 2019a) and Ukritchon and Keawsawasvong (2016, 2017a, b, c, 2018c, d, 2019f) while an in-house FELA code of the authors was also developed and applied (Keawsawasvong and Ukritchon, 2019b; Ukritchon and Keawsawasvong, 2018a, b, 2019b, c, d, e; Ukritchon et al., 2018, 2019, 2020).

It is worth noting that the recent authors' developments of LB FELA for the stability of rock masses (Ukritchon and Keawsawasvong, 2018b, 2019b, c) have a limitation in that a modified Hoek-Brown failure criterion with the exponential term $a = 0.5$ is employed. Thus, OputmG2 is adopted in the present study as the failure of rock masses can be modelled more correctly by the GHB criterion with any value of $a$ calculated from Eq. (4). In other words, there is no need to assume the exponential term $a = 0.5$ in OptumG2. Consequently, the numerical solutions of the problem can be accurately computed. In addition, the investigation for the stability of circular tunnels and the development of the new design equation of the problem are performed in the present study for the first time.

The followings summarize the calculations of UB and LB FELA using OptumG2 employed in the present study.

For the calculations of UB FELA, the soil mass is discretized by employing six-noded triangular elements whose nodes are associated with unknown velocity components that employ a quadratic interpolation within elements. The upper bound solution of the problem is obtained by solving the optimization problem that minimizes the surcharge ($\sigma_s$) (i.e., the objective function), and is subjected to the kinematically admissible velocity constraints including the compatibility and flow rule equations at triangular elements and velocity boundary conditions. The surcharge ($\sigma_s$) is linked with the unknown velocities of the problem through the principle of virtual work by equating the rate of work done by external loads with the internal energy dissipation at triangular elements.

For the calculations of LB FELA, the soil mass is discretized by employing three-noded triangular elements whose nodes are associated with unknown stress components that employ a linear interpolation within elements. In the lower bound mesh, stress discontinuities are introduced at shared edges of adjacent triangular elements by enabling nodes to be unique to elements. The lower bound solution of the problem is obtained by solving the optimization problem that maximizes the surcharge ($\sigma_s$) (i.e., the objective function), and is subjected to the statically admissible stress constraints including equilibrium equations within triangular elements and along stress discontinuities, stress boundary conditions, and no violation of the GHB failure criterion.

It should be noted that the present study focuses on the investigation for the stability of circular tunnels in rock masses and the development of a new design equation of the problem, while the details of numerical modeling of UB and LB FELA are not within the scope of the study. Readers are referred to the details of the method of limit analysis in Chen and Liu (1990) while those of numerical modelling of UB and LB FELA can be found in Sloan (2013) and Krabbenhoft et al. (2015).

It should be noted that different numbers of nodes per elements are used in UB and LB calculations, where the former employs six-noded elements while the latter employs three-noded ones. This is because the six-noded UB elements give rise to a linear variation of strain field, and produce a more accurate UB solution than using three-noded UB elements (Sloan, 2013; Krabbenhoft et al., 2015). In other words, three-noded UB elements generate a constant strain field that performs less accurately as compared with six-noded ones. Note that strict UB solutions can be computed by using both six-noded and three-noded UB elements. The three-noded LB element is the standard type of lower bound calculations that produce a linear variation of stress field and a strict LB solution. Six-noded LB elements have never developed in the research field of finite element limit analysis as they produce a non-rigorous LB solution of stability problems.

For both UB and LB simulations, the mesh adaptivity (e.g., Ciria et al., 2008), which is another power feature in OptumG2, is employed to compute the tight UB and LB solutions. For each iteration, a number of elements are automatically added in the zones that contain large plastic shear strain. The differences between UB and LB solutions at any iteration step are subsequently decreased by the mesh adaptivity feature, and hence, they converge to the true solution from above and below, respectively. If the setting of mesh adaptivity is adequate enough, suitable accurate solutions can be achieved. In all simulations otherwise stated, the setting of mesh adaptivity employs the initial mesh of a certain element that increases to a final mesh of a target element by five successive iterations. The initial and target elements are chosen approximately based on a trial-and-error study of some simulations as mentioned later such that the differences between UB and LB solution are within an acceptable limit of 5% or better.

## Verification

Even though the UB and LB FELA using OptumG2 (Krabbenhoft et al., 2015) have been successfully employed to investigate various stability problems by several researchers, their applications are mostly concentrated on Tresca and/or Mohr-Coulomb failure criteria (Keawsawasvong and Ukritchon, 2016a, b, 2017a, b, c, d, e, 2019a; Ukritchon and Keawsawasvong, 2016, 2017a, b, c, 2018c, d, 2019f). It should be noted that their applications to rock engineering problems are rather limited in the literature (Xiao et al., 2018) while their verification using the HB failure criterion is still not presented in that reference. To ensure the performance of the adopted computational FELA, two problems including plane strain biaxial compression of rock specimens and bearing capacity of rough strip footings on weightless rocks are selected as the verification. Numerical models of both problems are shown in Figs. 2a and 3b, respectively. The first verification corresponds to the simulation of plane strain biaxial compression of rock specimens. Only one-quarter of the full model is employed due to the symmetry of this problem (see Fig. 2a). The symmetrical left and bottom planes of the domain are allowed to move only in the vertical direction and only in the horizontal direction, respectively. The constant lateral pressure ($\sigma_h$) is applied on the right plane of the domain whereas the constant vertical pressure ($q$) is applied on the top plane. Then, $q$ is maximized and minimized as the objective function of LB and UB simulations, respectively, where $q > \sigma_h$. The rock specimen is weightless, and the other input parameters of rock masses include $DF = 0$, $m_i = 10$ and 30, and $GSI = 40$, 60, 80, and 100. Note that the uniaxial compressive strength ($\sigma_{ci}$) of rock specimen is used to normalized $\sigma_h$ and $q$. In this verification, $\sigma_h/\sigma_{ci}$ is fixed as 2. In all analyses of LB and UB FELA, the number of elements of meshes is set to be approximately 100 elements.

The exact analytical solution for the problem can be derived from Eq. (1) for the prediction of $q/\sigma_{ci}$ as:

$$\frac{q}{\sigma_{ci}} = \frac{\sigma_h}{\sigma_{ci}} + \left( m_b \frac{\sigma_h}{\sigma_{ci}} + s \right)^a \tag{6}$$

In Table 1, the UB and LB solutions of $q/\sigma_{ci}$ obtained from FELA are compared with the exact solutions. It is found that excellent agreement can be achieved for all cases, where

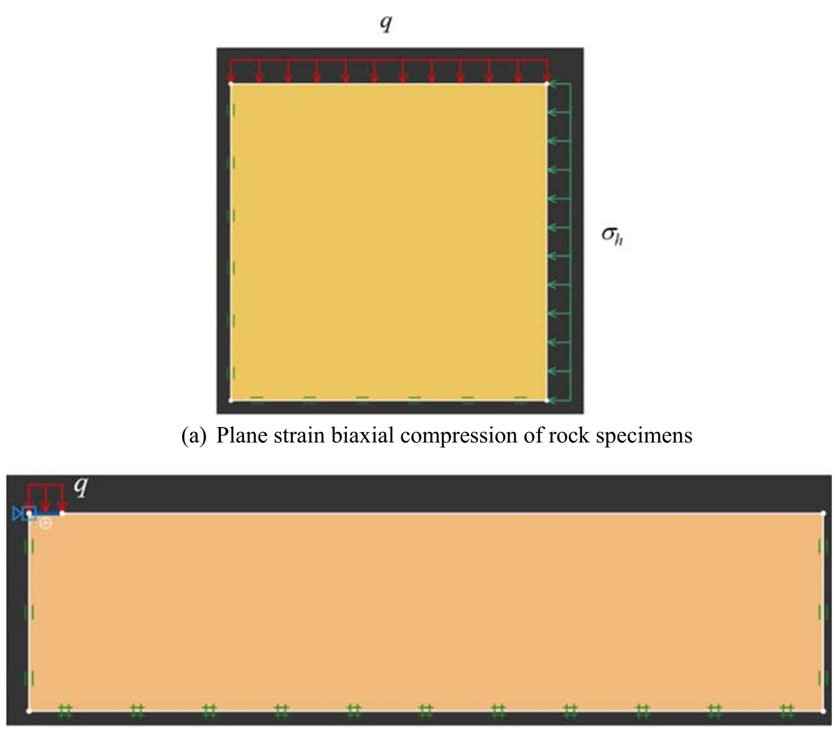


(a) Plane strain biaxial compression of rock specimens

(b) Strip footing

**Fig. 2** Numerical models of problem verification for the adopted FELA. **a** Plane strain biaxial compression of rock specimens. **b** Strip footing

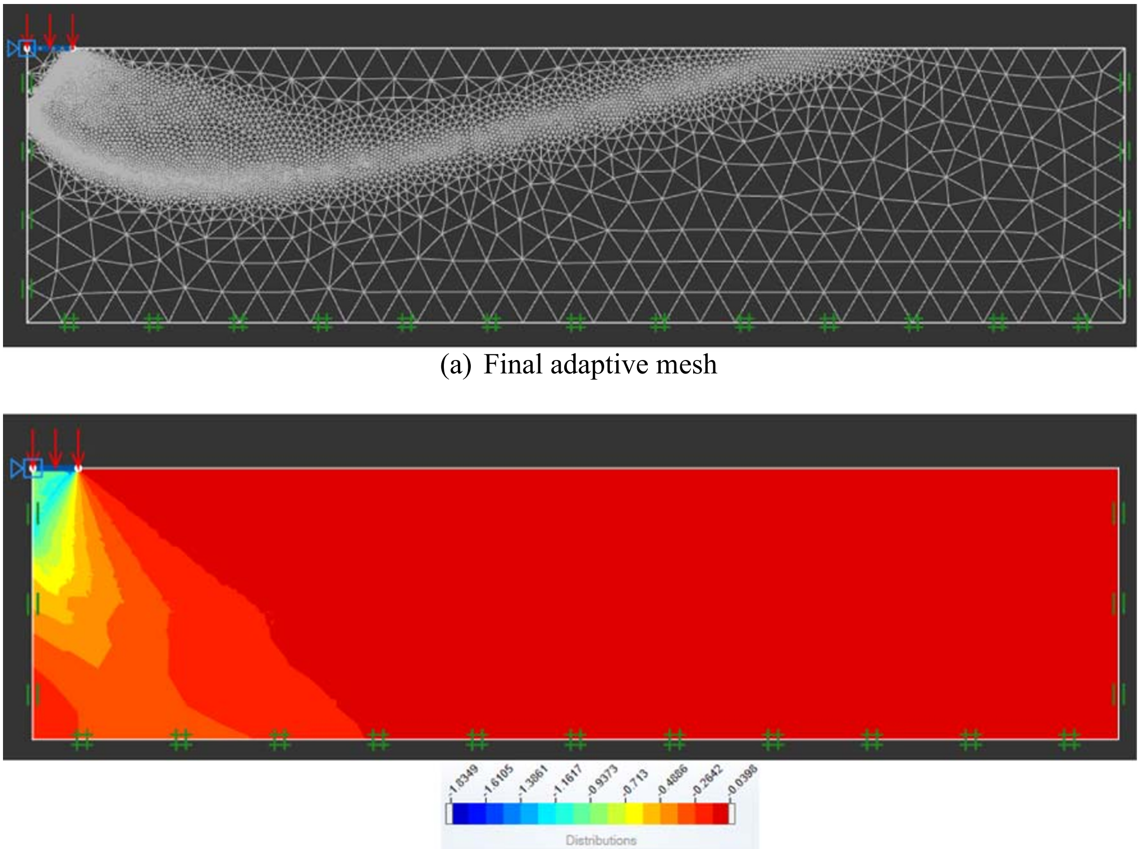


(a) Final adaptive mesh

(b) Stress contour of $\sigma_1/\sigma_{ci}$

**Fig. 3** Example results of strip footings on rock masses with $GSI = 50$ and $m_i = 10$. **a** Final adaptive mesh. **b** Stress contour of $\sigma_1/\sigma_{ci}$

the percent of difference between UB, LB, average (Avg) results, and the exact solutions is equal to zero for all cases. It should be noted that the feature of self-adaptive mesh refinement is not used in the biaxial compression of rock specimens since its exact solution is a constant state of stress and strain field. Hence, only coarse meshes are sufficiently enough to compute the accurate solutions. Closer inspections of stress and strain contours also confirm this observation. Since its stress field of rock specimen is a constant type and its failure mechanism is a uniform compression type with a uniform lateral spreading, such results are very trivial and are omitted for visual presentation.

The second verification corresponds to the bearing capacity of rough rigid strip footings on weightless rock masses. Only half of domain is selected in the analysis owing to the symmetry (see Fig. 2b). Only vertical movement is allowed at the symmetrical left plane. The bottom plane is enforced to be no movement in all directions while the right plane is constrained to be free movement in the vertical direction. The compressive load ($Q$) is applied under the footing. Beyond the edge of

**Table 1** Verification of the adopted FELA for the biaxial compression of rock specimens

| *GSI* | $m_i = 10$ | | | | | $m_i = 30$ | | | | |
|---|---|---|---|---|---|---|---|---|---|---|
| | UB<br>*q* | LB<br>*q* | Avg<br>*q* | Exact solution<br>*q* | % Diff. | UB<br>*q* | LB<br>*q* | Avg<br>*q* | Exact solution<br>*q* | % Diff. |
| 40 | 3.547 | 3.547 | 3.547 | 3.547 | 0.00 | 4.713 | 4.713 | 4.713 | 4.713 | 0.00 |
| 60 | 4.202 | 4.202 | 4.202 | 4.202 | 0.00 | 5.822 | 5.822 | 5.822 | 5.822 | 0.00 |
| 80 | 5.151 | 5.151 | 5.151 | 5.151 | 0.00 | 7.441 | 7.441 | 7.441 | 7.441 | 0.00 |
| 100 | 6.583 | 6.583 | 6.583 | 6.583 | 0.00 | 9.810 | 9.810 | 9.810 | 9.810 | 0.00 |

*Diff.* = difference

footing, the top surface is set to be free movement in both vertical and horizontal directions. The $Q$ load is maximized and minimized as the objective function of LB and UB simulations, respectively. The input material properties of rock masses are as follows: $DF = 0$, $m_i = 10$ and 30, $GSI = 50$. The initial number of elements is about 10,000 elements, and is then increased during five adaptive iterations, where the target number of elements is set to be about 50,000 elements. The bearing capacity factor ($N$) of footing is also represented as a dimensionless parameter as follows:

$$N = \frac{Q}{B\sigma_{ci}} = \frac{q}{\sigma_{ci}} \tag{7}$$

where $Q$ is the total vertical compressive load, $B$ is the full width of footing, $\sigma_{ci}$ is the uniaxial compressive strength of intact rock, and $q$ is the average pressure = $Q/A$.

Table 2 presents the comparison between all FELA results and the existing solutions of Merifield et al. (2006). Note that the computed bound solutions of each iteration during the mesh adaptivity are also reported in the table. At the first iteration, the percent of difference between the average bound solutions and the existing ones is quite high. However, at the fifth iteration, the excellent agreement between them can be observed, where the percent of the difference is less than 1% confirming the numerical accuracy of the simulations. Figure 3a shows the example of the final adaptive mesh (at 5th iteration). It can be seen that a number of elements significantly increase particularly in the area of failure zone. The contour of the dimensionless major principal stress $\sigma_1/\sigma_{ci}$ is also presented in Fig. 3b. It is found that the highest magnitude of the major principal stress takes place under the footing, and the magnitude then decreases when the contour is far from the edge of footing.

## Results and discussions of circular tunnels

The set of dimensionless parameters for shallow unlined circular tunnels in rock masses is described in Eq. (5). The

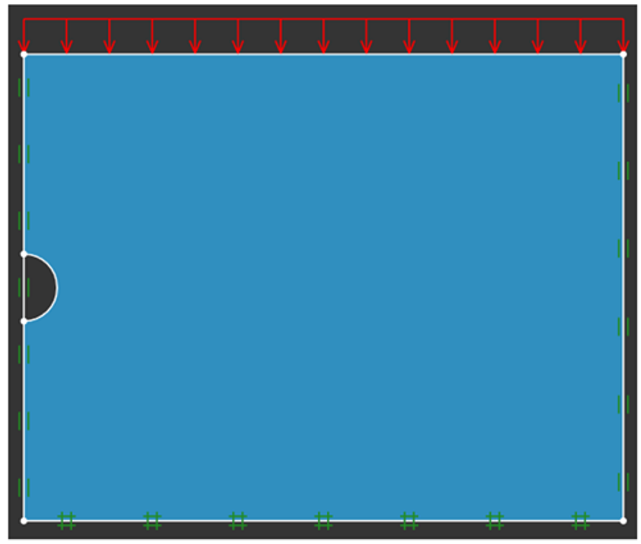

**Fig. 4** Numerical model of an infinitely long shallow unlined circular tunnel in a rock mass

shallow tunnels include the cover-depth ratio $C/D = 1$–5. The other dimensionless variables of the problem, namely $m_i$, $\sigma_{ci}/\gamma D$, and $GSI$, are considered as follows. First, the frictional strength of intact rock mass is studied in the range of $m_i = 5$–30 (as suggested by Hoek, 2004, 2007). In practice, the unit weight and uniaxial compressive strength for weak to strong rocks have the practical ranges of $\gamma = 22$–30 kN/m$^3$ and $\sigma_{ci} = 0.25$–250 MPa indicating that the normalized uniaxial compressive strength $\sigma_{ci}/\gamma D = 100$–$\infty$. Note that the case of $\sigma_{ci}/\gamma D = \infty$ corresponds to the case of rock masses that are extremely strong, where uniaxial compressive strength of rock is very large. Likewise, an extremely large value of $\sigma_{ci}/\gamma D$ also represents the theoretical case of weightless rock masses (i.e., $\gamma = 0$). This special case has been widely employed as one of setting inputs in various stability analyses of Hoek-Brown materials by many previous works (e.g., Chakraborty and Kumar, 2015; Kumar and Mohapatra, 2017; Merifield et al., 2006; Ukritchon and Keawsawasvong, 2018b, 2019b, c). Once the ranges of these dimensionless parameters are set up (e.g., $C/D = 1$–5, $\sigma_{ci}/\gamma D = 100$–$\infty$, and $m_i = 5$–30), the

**Table 2** Verification of the adopted FELA for the bearing capacity of strip footings on rock masses

| Adaptive iteration | $GSI = 50$, $m_i = 10$ | | | | | $GSI = 50$, $m_i = 30$ | | | | |
|---|---|---|---|---|---|---|---|---|---|---|
| | Present study | | | | Merifield et al. (2006) | Present study | | | | Merifield et al. (2006) |
| | UB $N_c$ | LB $N_c$ | Avg $N_c$ | % Diff.[a] | Avg $N_c$ | UB | LB | Avg $N_c$ | % Diff.[a] | Avg $N_c$ |
| 1st iteration | 1.134 | 0.774 | 0.954 | 8.32 | 1.037 | 2.973 | 1.405 | 2.189 | 11.94 | 2.467 |
| 3rd iteration | 1.074 | 0.946 | 1.010 | 2.64 | | 2.632 | 2.138 | 2.385 | 3.38 | |
| 5th iteration | 1.063 | 1.010 | 1.037 | 0.05 | | 2.551 | 2.343 | 2.447 | 0.81 | |

*Diff.* = difference

[a] The percentage difference of $N_c$ between the present study and Merifield et al. (2006)

**Table 3** Accuracy of self-adaptive refinement strategy, where $\sigma_{ci}/\gamma D = \infty$, $m_i = 10$, $GSI = 60$

| Number of adaptive iterations | Target number of elements | $C/D = 1$ | | | $C/D = 5$ | | |
|---|---|---|---|---|---|---|---|
| | | LB $\sigma_s/\sigma_{ci}$ | UB $\sigma_s/\sigma_{ci}$ | % Diff. | LB $\sigma_s/\sigma_{ci}$ | UB $\sigma_s/\sigma_{ci}$ | % Diff. |
| 3 | 5000 | 0.883 | 0.954 | 7.730 | 3.808 | 4.048 | 6.11 |
| | 10,000 | 0.895 | 0.946 | 5.540 | 3.834 | 4.040 | 5.23 |
| | 15,000 | 0.900 | 0.943 | 4.666 | 3.844 | 4.036 | 4.87 |
| 5 | 5000 | 0.892 | 0.946 | 5.876 | 3.844 | 4.043 | 5.05 |
| | 10,000 | 0.903 | 0.942 | 4.228 | 3.887 | 4.030 | 3.61 |
| | 15,000 | 0.907 | 0.940 | 3.573 | 3.901 | 4.024 | 3.10 |

*Diff.* = difference

feasible solutions of the problem can be successfully found by limiting the range of $GSI = 40$–$100$. If $GSI$ is less than 40, it is not possible to numerically compute the limiting surcharge of circular tunnel since the problem is initially failed by insufficient strengths of rock masses before applying any surcharge on the ground surface.

The numerical model of an infinitely long shallow unlined circular tunnel in a rock mass is shown in Fig. 4. Due to the symmetry of the problem, only half of the domain is used in numerical analyses (see Figs. 1 and 4). The boundary condition of the problem is defined such that the left plane of symmetry and the right plane are allow to move only in the vertical direction whereas the bottom plane is fixed in both vertical and horizontal directions. The uniform surcharge $\sigma_s$ is applied downward on the rock surface. Tunnel pressure is not considered inside the tunnel, and hence, there is no constraint in any direction along its circumferential free surface. In order to avoid any error in the computed bound solutions due to the problem size, the sizes of the domain are chosen to be so large that there is no intersection of plastic shear zone at the right and bottom boundaries. The UB and LB simulations of the collapse surcharge at the rock surface above circular tunnels are performed by minimizing and maximizing the loading multiplier on $\sigma_s$ for a given set of dimensionless parameters as presented in Eq. (5), respectively.

Table 3 shows the convergence and sensitivity study of the numerical modeling that examines two important factors affecting the accuracy of self-adaptive refinement feature in FELA, namely the target number of elements of 5000, 10,000, and 15,000 and the number of iterations of 3 and 5. In this study, circular tunnels with $C/D = 1$, 5, $\sigma_{ci}/\gamma D = \infty$, $m_i = 10$, and $GSI = 60$ are simulated, while the initial number of elements is fixed as 5000. Generally, the differences between UB and LB solutions can be decreased by employing the mesh adaptivity feature. It can be observed that the convergence of the computed UB and LB solutions of $\sigma_s/\sigma_{ci}$ can be generally found by increasing the target number of elements and the number of adaptive iterations. In addition, both solutions can be accurately improved by raising those two factors. Based on the results in Table 3, five iterations of adaptive meshing with the number of elements increasing from 5000 to 10,000 are employed in FELA simulations of circular tunnels in rock masses as this setting provides suitable accurate UB and LB solutions with reasonable computational time. Note that a setting of five adaptive iterations with 15,000 target elements is not selected because of its excessively long computational time during simulations.

Table 4 summarizes 320 computed UB and LB solutions of the normalized failure surcharge $\sigma_s/\sigma_{ci}$ of shallow unlined circular tunnels in Hoek-Brown rock masses. For all numerical results as reported in Table 4, the differences between UB and LB solutions are bracketed within 5% with respect to their averages. Figures 5, 6, 7, and 8 demonstrate some selected solutions to portray the effect of Hoek-Brown parameters on the stability of circular tunnels. It should be noted that all of computed results cannot be presented by the graphical plots in Figs. 5, 6, 7, and 8 due to the limited space of the paper. Thus, only some selected cases are graphically plotted in those figures. The dash lines in Figs. 5, 6, 7, and 8 represent the solutions of UB simulations whereas the solid lines illustrate those of LB ones. In Fig. 5, the impact of cover-depth ratio $C/D$ is investigated, which plots it in the horizontal axis of the figure while the normalized failure surcharge $\sigma_s/\sigma_{ci}$ is plotted in the vertical axis. The $GSI$ parameters in Fig. 5a, b, c, and d are equal to 40, 60, 80, and 100, respectively, and the normalized uniaxial strength of rock $\sigma_{ci}/\gamma D$ is fixed to be equal to 1000. The contour lines in Fig. 5a–d correspond to the $m_i$ variation of 10–30. It is found that the tendency of all lines in Fig. 5 shows a nonlinear relationship between $\sigma_s/\sigma_{ci}$ and $C/D$. This implies that the tunnels with a larger $C/D$ ratio have a higher stability than those with a smaller one. Figure 6 displays the influence of $GSI$ varying from 40 to 100 on the normalized failure surcharge $\sigma_s/\sigma_{ci}$, where $\sigma_{ci}/\gamma D$ is fixed to be equal to 500, and $C/D$ is varied as 1, 2, 3, 4, and 5. In addition, Fig. 6a, b, c, and d correspond to the cases of $m_i = 5$, 10, 20, and 30, respectively. The exponentially nonlinear relationship

**Table 4** Computed bound solutions of $\sigma_s/\sigma_{ci}$ for unlined circular tunnels in rock masses (pattern 1 is "slip line originates from the tunnel wall", and pattern 2 is "slip line originates below the tunnel base")

| $\sigma_{ci}/\gamma H$ | $GSI$ | $m_i$ | $C/H$ | $\sigma_s/\sigma_{ci}$ (LB) | $\sigma_s/\sigma_{ci}$ (UB) | $\sigma_s/\sigma_{ci}$ (Avg) | % diff | Pattern |
|---|---|---|---|---|---|---|---|---|
| 100 | 40 | 5 | 1 | 0.196 | 0.204 | 0.200 | 4.00 | 1 |
| 100 | 40 | 5 | 2 | 0.400 | 0.415 | 0.408 | 3.68 | 2 |
| 100 | 40 | 5 | 3 | 0.573 | 0.596 | 0.585 | 3.93 | 2 |
| 100 | 40 | 5 | 4 | 0.720 | 0.747 | 0.734 | 3.68 | 2 |
| 100 | 40 | 5 | 5 | 0.847 | 0.880 | 0.864 | 3.82 | 2 |
| 100 | 40 | 10 | 1 | 0.376 | 0.392 | 0.384 | 4.17 | 1 |
| 100 | 40 | 10 | 2 | 0.793 | 0.830 | 0.812 | 4.56 | 2 |
| 100 | 40 | 10 | 3 | 1.146 | 1.202 | 1.174 | 4.77 | 2 |
| 100 | 40 | 10 | 4 | 1.456 | 1.522 | 1.489 | 4.43 | 2 |
| 100 | 40 | 10 | 5 | 1.720 | 1.802 | 1.761 | 4.66 | 2 |
| 100 | 40 | 20 | 1 | 0.754 | 0.792 | 0.773 | 4.92 | 1 |
| 100 | 40 | 20 | 2 | 1.621 | 1.689 | 1.655 | 4.11 | 2 |
| 100 | 40 | 20 | 3 | 2.349 | 2.454 | 2.402 | 4.37 | 2 |
| 100 | 40 | 20 | 4 | 2.980 | 3.114 | 3.047 | 4.40 | 2 |
| 100 | 40 | 20 | 5 | 3.531 | 3.701 | 3.616 | 4.70 | 2 |
| 100 | 40 | 30 | 1 | 1.166 | 1.199 | 1.183 | 2.79 | 1 |
| 100 | 40 | 30 | 2 | 2.499 | 2.564 | 2.532 | 2.57 | 2 |
| 100 | 40 | 30 | 3 | 3.569 | 3.733 | 3.651 | 4.49 | 2 |
| 100 | 40 | 30 | 4 | 4.645 | 4.745 | 4.695 | 2.13 | 2 |
| 100 | 40 | 30 | 5 | 5.531 | 5.641 | 5.586 | 1.97 | 2 |
| 100 | 60 | 5 | 1 | 0.496 | 0.514 | 0.505 | 3.56 | 1 |
| 100 | 60 | 5 | 2 | 0.973 | 1.000 | 0.987 | 2.74 | 2 |
| 100 | 60 | 5 | 3 | 1.369 | 1.426 | 1.398 | 4.08 | 2 |
| 100 | 60 | 5 | 4 | 1.706 | 1.776 | 1.741 | 4.02 | 2 |
| 100 | 60 | 5 | 5 | 2.001 | 2.080 | 2.041 | 3.87 | 2 |
| 100 | 60 | 10 | 1 | 0.881 | 0.922 | 0.902 | 4.55 | 1 |
| 100 | 60 | 10 | 2 | 1.796 | 1.870 | 1.833 | 4.04 | 2 |
| 100 | 60 | 10 | 3 | 2.550 | 2.652 | 2.601 | 3.92 | 2 |
| 100 | 60 | 10 | 4 | 3.230 | 3.335 | 3.283 | 3.20 | 2 |
| 100 | 60 | 10 | 5 | 3.809 | 3.954 | 3.882 | 3.74 | 2 |
| 100 | 60 | 20 | 1 | 1.666 | 1.741 | 1.704 | 4.40 | 1 |
| 100 | 60 | 20 | 2 | 3.448 | 3.607 | 3.528 | 4.51 | 2 |
| 100 | 60 | 20 | 3 | 4.975 | 5.215 | 5.095 | 4.71 | 2 |
| 100 | 60 | 20 | 4 | 6.301 | 6.567 | 6.434 | 4.13 | 2 |
| 100 | 60 | 20 | 5 | 7.449 | 7.778 | 7.614 | 4.32 | 2 |
| 100 | 60 | 30 | 1 | 2.472 | 2.577 | 2.525 | 4.16 | 1 |
| 100 | 60 | 30 | 2 | 5.114 | 5.364 | 5.239 | 4.77 | 2 |
| 100 | 60 | 30 | 3 | 7.402 | 7.762 | 7.582 | 4.75 | 2 |
| 100 | 60 | 30 | 4 | 9.380 | 9.739 | 9.560 | 3.76 | 2 |
| 100 | 60 | 30 | 5 | 11.240 | 11.540 | 11.390 | 2.63 | 2 |
| 100 | 80 | 5 | 1 | 1.173 | 1.214 | 1.194 | 3.44 | 1 |
| 100 | 80 | 5 | 2 | 2.228 | 2.285 | 2.257 | 2.53 | 2 |
| 100 | 80 | 5 | 3 | 3.079 | 3.212 | 3.146 | 4.23 | 2 |
| 100 | 80 | 5 | 4 | 3.824 | 3.922 | 3.873 | 2.53 | 2 |
| 100 | 80 | 5 | 5 | 4.457 | 4.615 | 4.536 | 3.48 | 2 |
| 100 | 80 | 10 | 1 | 1.967 | 2.063 | 2.015 | 4.76 | 1 |
| 100 | 80 | 10 | 2 | 3.925 | 4.103 | 4.014 | 4.43 | 2 |

**Table 4** (continued)

| $\sigma_{ci}/\gamma H$ | $GSI$ | $m_i$ | $C/H$ | $\sigma_s/\sigma_{ci}$ (LB) | $\sigma_s/\sigma_{ci}$ (UB) | $\sigma_s/\sigma_{ci}$ (Avg) | % diff | Pattern |
|---|---|---|---|---|---|---|---|---|
| 100 | 80 | 10 | 3 | 5.540 | 5.789 | 5.665 | 4.40 | 2 |
| 100 | 80 | 10 | 4 | 6.943 | 7.256 | 7.100 | 4.41 | 2 |
| 100 | 80 | 10 | 5 | 8.146 | 8.515 | 8.331 | 4.43 | 2 |
| 100 | 80 | 20 | 1 | 3.549 | 3.727 | 3.638 | 4.89 | 1 |
| 100 | 80 | 20 | 2 | 7.301 | 7.614 | 7.458 | 4.20 | 2 |
| 100 | 80 | 20 | 3 | 10.444 | 10.781 | 10.613 | 3.18 | 2 |
| 100 | 80 | 20 | 4 | 13.117 | 13.578 | 13.348 | 3.45 | 2 |
| 100 | 80 | 20 | 5 | 15.542 | 16.041 | 15.792 | 3.16 | 2 |
| 100 | 80 | 30 | 1 | 5.231 | 5.400 | 5.316 | 3.18 | 1 |
| 100 | 80 | 30 | 2 | 10.675 | 11.076 | 10.876 | 3.69 | 2 |
| 100 | 80 | 30 | 3 | 15.347 | 15.879 | 15.613 | 3.41 | 2 |
| 100 | 80 | 30 | 4 | 19.342 | 20.053 | 19.698 | 3.61 | 2 |
| 100 | 80 | 30 | 5 | 22.837 | 23.711 | 23.274 | 3.76 | 2 |
| 100 | 100 | 5 | 1 | 2.788 | 2.875 | 2.832 | 3.07 | 1 |
| 100 | 100 | 5 | 2 | 5.140 | 5.283 | 5.212 | 2.74 | 2 |
| 100 | 100 | 5 | 3 | 7.032 | 7.246 | 7.139 | 3.00 | 2 |
| 100 | 100 | 5 | 4 | 8.610 | 8.899 | 8.755 | 3.30 | 2 |
| 100 | 100 | 5 | 5 | 9.997 | 10.314 | 10.156 | 3.12 | 2 |
| 100 | 100 | 10 | 1 | 4.425 | 4.570 | 4.498 | 3.22 | 1 |
| 100 | 100 | 10 | 2 | 8.566 | 8.916 | 8.741 | 4.00 | 2 |
| 100 | 100 | 10 | 3 | 12.042 | 12.526 | 12.284 | 3.94 | 2 |
| 100 | 100 | 10 | 4 | 14.979 | 15.367 | 15.173 | 2.56 | 2 |
| 100 | 100 | 10 | 5 | 17.424 | 17.994 | 17.709 | 3.22 | 2 |
| 100 | 100 | 20 | 1 | 7.689 | 8.042 | 7.866 | 4.49 | 1 |
| 100 | 100 | 20 | 2 | 15.468 | 15.932 | 15.700 | 2.96 | 2 |
| 100 | 100 | 20 | 3 | 22.026 | 22.703 | 22.365 | 3.03 | 2 |
| 100 | 100 | 20 | 4 | 27.654 | 28.506 | 28.080 | 3.03 | 2 |
| 100 | 100 | 20 | 5 | 32.515 | 33.569 | 33.042 | 3.19 | 2 |
| 100 | 100 | 30 | 1 | 10.966 | 11.491 | 11.229 | 4.68 | 1 |
| 100 | 100 | 30 | 2 | 22.316 | 23.117 | 22.717 | 3.53 | 2 |
| 100 | 100 | 30 | 3 | 31.988 | 33.027 | 32.508 | 3.20 | 2 |
| 100 | 100 | 30 | 4 | 40.265 | 41.361 | 40.813 | 2.69 | 2 |
| 100 | 100 | 30 | 5 | 47.457 | 48.833 | 48.145 | 2.86 | 2 |
| 500 | 40 | 5 | 1 | 0.213 | 0.220 | 0.217 | 3.23 | 1 |
| 500 | 40 | 5 | 2 | 0.429 | 0.446 | 0.438 | 3.89 | 2 |
| 500 | 40 | 5 | 3 | 0.613 | 0.635 | 0.624 | 3.53 | 2 |
| 500 | 40 | 5 | 4 | 0.771 | 0.800 | 0.786 | 3.69 | 2 |
| 500 | 40 | 5 | 5 | 0.910 | 0.944 | 0.927 | 3.67 | 2 |
| 500 | 40 | 10 | 1 | 0.393 | 0.412 | 0.403 | 4.72 | 1 |
| 500 | 40 | 10 | 2 | 0.837 | 0.863 | 0.850 | 3.06 | 2 |
| 500 | 40 | 10 | 3 | 1.192 | 1.246 | 1.219 | 4.43 | 2 |
| 500 | 40 | 10 | 4 | 1.510 | 1.572 | 1.541 | 4.02 | 2 |
| 500 | 40 | 10 | 5 | 1.791 | 1.866 | 1.829 | 4.10 | 2 |
| 500 | 40 | 20 | 1 | 0.793 | 0.811 | 0.802 | 2.24 | 1 |
| 500 | 40 | 20 | 2 | 1.638 | 1.720 | 1.679 | 4.88 | 2 |
| 500 | 40 | 20 | 3 | 2.384 | 2.496 | 2.440 | 4.59 | 2 |
| 500 | 40 | 20 | 4 | 3.021 | 3.161 | 3.091 | 4.53 | 2 |
| 500 | 40 | 20 | 5 | 3.598 | 3.759 | 3.679 | 4.38 | 2 |

**Table 4** (continued)

| $\sigma_{ci}/\gamma H$ | $GSI$ | $m_i$ | $C/H$ | $\sigma_s/\sigma_{ci}$ (LB) | $\sigma_s/\sigma_{ci}$ (UB) | $\sigma_s/\sigma_{ci}$ (Avg) | % diff | Pattern |
|---|---|---|---|---|---|---|---|---|
| 500 | 40 | 30 | 1 | 1.184 | 1.217 | 1.201 | 2.75 | 1 |
| 500 | 40 | 30 | 2 | 2.469 | 2.590 | 2.530 | 4.78 | 2 |
| 500 | 40 | 30 | 3 | 3.593 | 3.777 | 3.685 | 4.99 | 2 |
| 500 | 40 | 30 | 4 | 4.562 | 4.793 | 4.678 | 4.94 | 2 |
| 500 | 40 | 30 | 5 | 5.441 | 5.702 | 5.572 | 4.68 | 2 |
| 500 | 60 | 5 | 1 | 0.509 | 0.535 | 0.522 | 4.98 | 1 |
| 500 | 60 | 5 | 2 | 1.000 | 1.046 | 1.023 | 4.50 | 2 |
| 500 | 60 | 5 | 3 | 1.404 | 1.465 | 1.435 | 4.25 | 2 |
| 500 | 60 | 5 | 4 | 1.753 | 1.834 | 1.794 | 4.52 | 2 |
| 500 | 60 | 5 | 5 | 2.058 | 2.141 | 2.100 | 3.95 | 2 |
| 500 | 60 | 10 | 1 | 0.899 | 0.937 | 0.918 | 4.14 | 1 |
| 500 | 60 | 10 | 2 | 1.827 | 1.898 | 1.863 | 3.81 | 2 |
| 500 | 60 | 10 | 3 | 2.608 | 2.702 | 2.655 | 3.54 | 2 |
| 500 | 60 | 10 | 4 | 3.278 | 3.404 | 3.341 | 3.77 | 2 |
| 500 | 60 | 10 | 5 | 3.879 | 3.997 | 3.938 | 3.00 | 2 |
| 500 | 60 | 20 | 1 | 1.687 | 1.759 | 1.723 | 4.18 | 1 |
| 500 | 60 | 20 | 2 | 3.488 | 3.654 | 3.571 | 4.65 | 2 |
| 500 | 60 | 20 | 3 | 5.022 | 5.240 | 5.131 | 4.25 | 2 |
| 500 | 60 | 20 | 4 | 6.350 | 6.630 | 6.490 | 4.31 | 2 |
| 500 | 60 | 20 | 5 | 7.512 | 7.821 | 7.667 | 4.03 | 2 |
| 500 | 60 | 30 | 1 | 2.482 | 2.597 | 2.540 | 4.53 | 1 |
| 500 | 60 | 30 | 2 | 5.205 | 5.400 | 5.303 | 3.68 | 2 |
| 500 | 60 | 30 | 3 | 7.457 | 7.792 | 7.625 | 4.39 | 2 |
| 500 | 60 | 30 | 4 | 9.439 | 9.798 | 9.619 | 3.73 | 2 |
| 500 | 60 | 30 | 5 | 11.128 | 11.617 | 11.373 | 4.30 | 2 |
| 500 | 80 | 5 | 1 | 1.187 | 1.233 | 1.210 | 3.80 | 1 |
| 500 | 80 | 5 | 2 | 2.253 | 2.341 | 2.297 | 3.83 | 2 |
| 500 | 80 | 5 | 3 | 3.120 | 3.243 | 3.182 | 3.87 | 2 |
| 500 | 80 | 5 | 4 | 3.867 | 4.022 | 3.945 | 3.93 | 2 |
| 500 | 80 | 5 | 5 | 4.514 | 4.670 | 4.592 | 3.40 | 2 |
| 500 | 80 | 10 | 1 | 1.983 | 2.078 | 2.031 | 4.68 | 1 |
| 500 | 80 | 10 | 2 | 3.946 | 4.103 | 4.025 | 3.90 | 2 |
| 500 | 80 | 10 | 3 | 5.581 | 5.833 | 5.707 | 4.42 | 2 |
| 500 | 80 | 10 | 4 | 6.975 | 7.299 | 7.137 | 4.54 | 2 |
| 500 | 80 | 10 | 5 | 8.207 | 8.546 | 8.377 | 4.05 | 2 |
| 500 | 80 | 20 | 1 | 3.570 | 3.749 | 3.660 | 4.89 | 1 |
| 500 | 80 | 20 | 2 | 7.313 | 7.650 | 7.482 | 4.50 | 2 |
| 500 | 80 | 20 | 3 | 10.484 | 10.837 | 10.661 | 3.31 | 2 |
| 500 | 80 | 20 | 4 | 13.205 | 13.642 | 13.424 | 3.26 | 2 |
| 500 | 80 | 20 | 5 | 15.609 | 16.108 | 15.859 | 3.15 | 2 |
| 500 | 80 | 30 | 1 | 5.182 | 5.432 | 5.307 | 4.71 | 1 |
| 500 | 80 | 30 | 2 | 10.667 | 11.154 | 10.911 | 4.46 | 2 |
| 500 | 80 | 30 | 3 | 15.358 | 15.926 | 15.642 | 3.63 | 2 |
| 500 | 80 | 30 | 4 | 19.407 | 20.117 | 19.762 | 3.59 | 2 |
| 500 | 80 | 30 | 5 | 22.942 | 23.779 | 23.361 | 3.58 | 2 |
| 500 | 100 | 5 | 1 | 2.828 | 2.894 | 2.861 | 2.31 | 1 |
| 500 | 100 | 5 | 2 | 5.169 | 5.306 | 5.238 | 2.62 | 2 |
| 500 | 100 | 5 | 3 | 7.059 | 7.264 | 7.162 | 2.86 | 2 |

**Table 4** (continued)

| $\sigma_{ci}/\gamma H$ | $GSI$ | $m_i$ | $C/H$ | $\sigma_s/\sigma_{ci}$ (LB) | $\sigma_s/\sigma_{ci}$ (UB) | $\sigma_s/\sigma_{ci}$ (Avg) | % diff | Pattern |
|---|---|---|---|---|---|---|---|---|
| 500 | 100 | 5 | 4 | 8.657 | 8.943 | 8.800 | 3.25 | 2 |
| 500 | 100 | 5 | 5 | 10.059 | 10.390 | 10.225 | 3.24 | 2 |
| 500 | 100 | 10 | 1 | 4.448 | 4.563 | 4.506 | 2.55 | 1 |
| 500 | 100 | 10 | 2 | 8.609 | 8.954 | 8.782 | 3.93 | 2 |
| 500 | 100 | 10 | 3 | 12.051 | 12.583 | 12.317 | 4.32 | 2 |
| 500 | 100 | 10 | 4 | 14.992 | 15.672 | 15.332 | 4.44 | 2 |
| 500 | 100 | 10 | 5 | 17.590 | 18.067 | 17.829 | 2.68 | 2 |
| 500 | 100 | 20 | 1 | 7.699 | 8.076 | 7.888 | 4.78 | 1 |
| 500 | 100 | 20 | 2 | 15.496 | 15.969 | 15.733 | 3.01 | 2 |
| 500 | 100 | 20 | 3 | 22.084 | 22.766 | 22.425 | 3.04 | 2 |
| 500 | 100 | 20 | 4 | 27.718 | 28.538 | 28.128 | 2.92 | 2 |
| 500 | 100 | 20 | 5 | 32.631 | 33.623 | 33.127 | 2.99 | 2 |
| 500 | 100 | 30 | 1 | 10.990 | 11.512 | 11.251 | 4.64 | 1 |
| 500 | 100 | 30 | 2 | 22.373 | 23.114 | 22.744 | 3.26 | 2 |
| 500 | 100 | 30 | 3 | 31.844 | 33.139 | 32.492 | 3.99 | 2 |
| 500 | 100 | 30 | 4 | 40.284 | 41.454 | 40.869 | 2.86 | 2 |
| 500 | 100 | 30 | 5 | 47.523 | 48.933 | 48.228 | 2.92 | 2 |
| 1000 | 40 | 5 | 1 | 0.214 | 0.223 | 0.219 | 4.12 | 1 |
| 1000 | 40 | 5 | 2 | 0.429 | 0.449 | 0.439 | 4.56 | 2 |
| 1000 | 40 | 5 | 3 | 0.619 | 0.640 | 0.630 | 3.34 | 2 |
| 1000 | 40 | 5 | 4 | 0.778 | 0.807 | 0.793 | 3.66 | 2 |
| 1000 | 40 | 5 | 5 | 0.918 | 0.953 | 0.936 | 3.74 | 2 |
| 1000 | 40 | 10 | 1 | 0.397 | 0.415 | 0.406 | 4.43 | 1 |
| 1000 | 40 | 10 | 2 | 0.829 | 0.867 | 0.848 | 4.48 | 2 |
| 1000 | 40 | 10 | 3 | 1.198 | 1.251 | 1.225 | 4.33 | 2 |
| 1000 | 40 | 10 | 4 | 1.518 | 1.580 | 1.549 | 4.00 | 2 |
| 1000 | 40 | 10 | 5 | 1.797 | 1.875 | 1.836 | 4.25 | 2 |
| 1000 | 40 | 20 | 1 | 0.782 | 0.815 | 0.799 | 4.13 | 1 |
| 1000 | 40 | 20 | 2 | 1.644 | 1.718 | 1.681 | 4.40 | 2 |
| 1000 | 40 | 20 | 3 | 2.392 | 2.505 | 2.449 | 4.62 | 2 |
| 1000 | 40 | 20 | 4 | 3.034 | 3.177 | 3.106 | 4.60 | 2 |
| 1000 | 40 | 20 | 5 | 3.611 | 3.769 | 3.690 | 4.28 | 2 |
| 1000 | 40 | 30 | 1 | 1.183 | 1.218 | 1.201 | 2.92 | 2 |
| 1000 | 40 | 30 | 2 | 2.483 | 2.594 | 2.539 | 4.37 | 2 |
| 1000 | 40 | 30 | 3 | 3.603 | 3.777 | 3.690 | 4.72 | 2 |
| 1000 | 40 | 30 | 4 | 4.581 | 4.806 | 4.694 | 4.79 | 2 |
| 1000 | 40 | 30 | 5 | 5.453 | 5.706 | 5.580 | 4.53 | 2 |
| 1000 | 60 | 5 | 1 | 0.513 | 0.536 | 0.525 | 4.39 | 1 |
| 1000 | 60 | 5 | 2 | 1.005 | 1.050 | 1.028 | 4.38 | 2 |
| 1000 | 60 | 5 | 3 | 1.412 | 1.470 | 1.441 | 4.02 | 2 |
| 1000 | 60 | 5 | 4 | 1.758 | 1.833 | 1.796 | 4.18 | 2 |
| 1000 | 60 | 5 | 5 | 2.059 | 2.147 | 2.103 | 4.18 | 2 |
| 1000 | 60 | 10 | 1 | 0.901 | 0.941 | 0.921 | 4.34 | 1 |
| 1000 | 60 | 10 | 2 | 1.822 | 1.902 | 1.862 | 4.30 | 2 |
| 1000 | 60 | 10 | 3 | 2.614 | 2.705 | 2.660 | 3.42 | 2 |
| 1000 | 60 | 10 | 4 | 3.289 | 3.410 | 3.350 | 3.61 | 2 |
| 1000 | 60 | 10 | 5 | 3.872 | 4.004 | 3.938 | 3.35 | 2 |
| 1000 | 60 | 20 | 1 | 1.697 | 1.763 | 1.730 | 3.82 | 1 |

**Table 4** (continued)

| $\sigma_{ci}/\gamma H$ | *GSI* | $m_i$ | *C/H* | $\sigma_s/\sigma_{ci}$ (LB) | $\sigma_s/\sigma_{ci}$ (UB) | $\sigma_s/\sigma_{ci}$ (Avg) | % diff | Pattern |
|---|---|---|---|---|---|---|---|---|
| 1000 | 60 | 20 | 2 | 3.494 | 3.657 | 3.576 | 4.56 | 2 |
| 1000 | 60 | 20 | 3 | 5.026 | 5.236 | 5.131 | 4.09 | 2 |
| 1000 | 60 | 20 | 4 | 6.359 | 6.602 | 6.481 | 3.75 | 2 |
| 1000 | 60 | 20 | 5 | 7.516 | 7.850 | 7.683 | 4.35 | 2 |
| 1000 | 60 | 30 | 1 | 2.499 | 2.599 | 2.549 | 3.92 | 2 |
| 1000 | 60 | 30 | 2 | 5.162 | 5.369 | 5.266 | 3.93 | 2 |
| 1000 | 60 | 30 | 3 | 7.439 | 7.756 | 7.598 | 4.17 | 2 |
| 1000 | 60 | 30 | 4 | 9.429 | 9.812 | 9.621 | 3.98 | 2 |
| 1000 | 60 | 30 | 5 | 11.174 | 11.594 | 11.384 | 3.69 | 2 |
| 1000 | 80 | 5 | 1 | 1.191 | 1.224 | 1.208 | 2.73 | 1 |
| 1000 | 80 | 5 | 2 | 2.255 | 2.341 | 2.298 | 3.74 | 2 |
| 1000 | 80 | 5 | 3 | 3.122 | 3.249 | 3.186 | 3.99 | 2 |
| 1000 | 80 | 5 | 4 | 3.873 | 4.020 | 3.947 | 3.72 | 2 |
| 1000 | 80 | 5 | 5 | 4.522 | 4.686 | 4.604 | 3.56 | 2 |
| 1000 | 80 | 10 | 1 | 1.998 | 2.080 | 2.039 | 4.02 | 1 |
| 1000 | 80 | 10 | 2 | 3.950 | 4.118 | 4.034 | 4.16 | 2 |
| 1000 | 80 | 10 | 3 | 5.592 | 5.832 | 5.712 | 4.20 | 2 |
| 1000 | 80 | 10 | 4 | 6.972 | 7.292 | 7.132 | 4.49 | 2 |
| 1000 | 80 | 10 | 5 | 8.212 | 8.566 | 8.389 | 4.22 | 2 |
| 1000 | 80 | 20 | 1 | 3.573 | 3.752 | 3.663 | 4.89 | 1 |
| 1000 | 80 | 20 | 2 | 7.328 | 7.676 | 7.502 | 4.64 | 2 |
| 1000 | 80 | 20 | 3 | 10.480 | 10.836 | 10.658 | 3.34 | 2 |
| 1000 | 80 | 20 | 4 | 13.175 | 13.645 | 13.410 | 3.50 | 2 |
| 1000 | 80 | 20 | 5 | 15.591 | 16.096 | 15.844 | 3.19 | 2 |
| 1000 | 80 | 30 | 1 | 5.141 | 5.386 | 5.264 | 4.65 | 2 |
| 1000 | 80 | 30 | 2 | 10.683 | 11.119 | 10.901 | 4.00 | 2 |
| 1000 | 80 | 30 | 3 | 15.343 | 15.950 | 15.647 | 3.88 | 2 |
| 1000 | 80 | 30 | 4 | 19.455 | 20.108 | 19.782 | 3.30 | 2 |
| 1000 | 80 | 30 | 5 | 22.993 | 23.745 | 23.369 | 3.22 | 2 |
| 1000 | 100 | 5 | 1 | 2.828 | 2.891 | 2.860 | 2.20 | 1 |
| 1000 | 100 | 5 | 2 | 5.177 | 5.287 | 5.232 | 2.10 | 2 |
| 1000 | 100 | 5 | 3 | 7.062 | 7.281 | 7.172 | 3.05 | 2 |
| 1000 | 100 | 5 | 4 | 8.670 | 8.940 | 8.805 | 3.07 | 2 |
| 1000 | 100 | 5 | 5 | 10.060 | 10.369 | 10.215 | 3.03 | 2 |
| 1000 | 100 | 10 | 1 | 4.454 | 4.582 | 4.518 | 2.83 | 1 |
| 1000 | 100 | 10 | 2 | 8.609 | 8.994 | 8.802 | 4.37 | 2 |
| 1000 | 100 | 10 | 3 | 12.069 | 12.570 | 12.320 | 4.07 | 2 |
| 1000 | 100 | 10 | 4 | 15.036 | 15.398 | 15.217 | 2.38 | 2 |
| 1000 | 100 | 10 | 5 | 17.591 | 18.050 | 17.821 | 2.58 | 2 |
| 1000 | 100 | 20 | 1 | 7.789 | 8.078 | 7.934 | 3.64 | 1 |
| 1000 | 100 | 20 | 2 | 15.507 | 15.990 | 15.749 | 3.07 | 2 |
| 1000 | 100 | 20 | 3 | 22.093 | 22.767 | 22.430 | 3.00 | 2 |
| 1000 | 100 | 20 | 4 | 27.717 | 28.544 | 28.131 | 2.94 | 2 |
| 1000 | 100 | 20 | 5 | 32.622 | 33.626 | 33.124 | 3.03 | 2 |
| 1000 | 100 | 30 | 1 | 10.997 | 11.483 | 11.240 | 4.32 | 2 |
| 1000 | 100 | 30 | 2 | 22.389 | 23.120 | 22.755 | 3.21 | 2 |
| 1000 | 100 | 30 | 3 | 32.057 | 33.071 | 32.564 | 3.11 | 2 |
| 1000 | 100 | 30 | 4 | 40.345 | 41.406 | 40.876 | 2.60 | 2 |

**Table 4** (continued)

| $\sigma_{ci}/\gamma H$ | $GSI$ | $m_i$ | $C/H$ | $\sigma_s/\sigma_{ci}$ (LB) | $\sigma_s/\sigma_{ci}$ (UB) | $\sigma_s/\sigma_{ci}$ (Avg) | % diff | Pattern |
|---|---|---|---|---|---|---|---|---|
| 1000 | 100 | 30 | 5 | 47.497 | 48.939 | 48.218 | 2.99 | 2 |
| ∞ | 40 | 5 | 1 | 0.232 | 0.224 | 0.228 | 3.51 | 1 |
| ∞ | 40 | 5 | 2 | 0.437 | 0.452 | 0.445 | 3.37 | 2 |
| ∞ | 40 | 5 | 3 | 0.623 | 0.647 | 0.635 | 3.78 | 2 |
| ∞ | 40 | 5 | 4 | 0.785 | 0.812 | 0.799 | 3.38 | 2 |
| ∞ | 40 | 5 | 5 | 0.924 | 0.958 | 0.941 | 3.61 | 2 |
| ∞ | 40 | 10 | 1 | 0.400 | 0.418 | 0.409 | 4.40 | 1 |
| ∞ | 40 | 10 | 2 | 0.833 | 0.869 | 0.851 | 4.23 | 2 |
| ∞ | 40 | 10 | 3 | 1.198 | 1.255 | 1.227 | 4.65 | 2 |
| ∞ | 40 | 10 | 4 | 1.525 | 1.589 | 1.557 | 4.11 | 2 |
| ∞ | 40 | 10 | 5 | 1.804 | 1.880 | 1.842 | 4.13 | 2 |
| ∞ | 40 | 20 | 1 | 0.791 | 0.814 | 0.803 | 2.87 | 1 |
| ∞ | 40 | 20 | 2 | 1.645 | 1.729 | 1.687 | 4.98 | 2 |
| ∞ | 40 | 20 | 3 | 2.396 | 2.512 | 2.454 | 4.73 | 2 |
| ∞ | 40 | 20 | 4 | 3.046 | 3.178 | 3.112 | 4.24 | 2 |
| ∞ | 40 | 20 | 5 | 3.617 | 3.779 | 3.698 | 4.38 | 2 |
| ∞ | 40 | 30 | 1 | 1.189 | 1.224 | 1.207 | 2.90 | 2 |
| ∞ | 40 | 30 | 2 | 2.479 | 2.598 | 2.539 | 4.69 | 2 |
| ∞ | 40 | 30 | 3 | 3.610 | 3.784 | 3.697 | 4.71 | 2 |
| ∞ | 40 | 30 | 4 | 4.588 | 4.817 | 4.703 | 4.87 | 2 |
| ∞ | 40 | 30 | 5 | 5.467 | 5.722 | 5.595 | 4.56 | 2 |
| ∞ | 60 | 5 | 1 | 0.514 | 0.539 | 0.527 | 4.75 | 1 |
| ∞ | 60 | 5 | 2 | 1.007 | 1.053 | 1.030 | 4.47 | 2 |
| ∞ | 60 | 5 | 3 | 1.416 | 1.477 | 1.447 | 4.22 | 2 |
| ∞ | 60 | 5 | 4 | 1.768 | 1.841 | 1.805 | 4.05 | 2 |
| ∞ | 60 | 5 | 5 | 2.075 | 2.153 | 2.114 | 3.69 | 2 |
| ∞ | 60 | 10 | 1 | 0.903 | 0.942 | 0.923 | 4.23 | 1 |
| ∞ | 60 | 10 | 2 | 1.833 | 1.905 | 1.869 | 3.85 | 2 |
| ∞ | 60 | 10 | 3 | 2.617 | 2.712 | 2.665 | 3.57 | 2 |
| ∞ | 60 | 10 | 4 | 3.299 | 3.413 | 3.356 | 3.40 | 2 |
| ∞ | 60 | 10 | 5 | 3.887 | 4.030 | 3.959 | 3.61 | 2 |
| ∞ | 60 | 20 | 1 | 1.698 | 1.771 | 1.735 | 4.21 | 1 |
| ∞ | 60 | 20 | 2 | 3.497 | 3.644 | 3.571 | 4.12 | 2 |
| ∞ | 60 | 20 | 3 | 5.039 | 5.243 | 5.141 | 3.97 | 2 |
| ∞ | 60 | 20 | 4 | 6.377 | 6.651 | 6.514 | 4.21 | 2 |
| ∞ | 60 | 20 | 5 | 7.528 | 7.846 | 7.687 | 4.14 | 2 |
| ∞ | 60 | 30 | 1 | 2.479 | 2.597 | 2.538 | 4.65 | 2 |
| ∞ | 60 | 30 | 2 | 5.154 | 5.400 | 5.277 | 4.66 | 2 |
| ∞ | 60 | 30 | 3 | 7.464 | 7.800 | 7.632 | 4.40 | 2 |
| ∞ | 60 | 30 | 4 | 9.449 | 9.899 | 9.674 | 4.65 | 2 |
| ∞ | 60 | 30 | 5 | 11.163 | 11.630 | 11.397 | 4.10 | 2 |
| ∞ | 80 | 5 | 1 | 1.191 | 1.220 | 1.206 | 2.41 | 1 |
| ∞ | 80 | 5 | 2 | 2.257 | 2.351 | 2.304 | 4.08 | 2 |
| ∞ | 80 | 5 | 3 | 3.140 | 3.218 | 3.179 | 2.45 | 2 |
| ∞ | 80 | 5 | 4 | 3.883 | 4.036 | 3.960 | 3.86 | 2 |
| ∞ | 80 | 5 | 5 | 4.517 | 4.692 | 4.605 | 3.80 | 2 |
| ∞ | 80 | 10 | 1 | 1.987 | 2.083 | 2.035 | 4.72 | 1 |
| ∞ | 80 | 10 | 2 | 3.949 | 4.124 | 4.037 | 4.34 | 2 |

**Table 4** (continued)

| $\sigma_{ci}/\gamma H$ | *GSI* | $m_i$ | *C/H* | $\sigma_s/\sigma_{ci}$ (LB) | $\sigma_s/\sigma_{ci}$ (UB) | $\sigma_s/\sigma_{ci}$ (Avg) | % diff | Pattern |
|---|---|---|---|---|---|---|---|---|
| ∞ | 80 | 10 | 3 | 5.602 | 5.833 | 5.718 | 4.04 | 2 |
| ∞ | 80 | 10 | 4 | 6.985 | 7.308 | 7.147 | 4.52 | 2 |
| ∞ | 80 | 10 | 5 | 8.243 | 8.575 | 8.409 | 3.95 | 2 |
| ∞ | 80 | 20 | 1 | 3.589 | 3.754 | 3.672 | 4.49 | 1 |
| ∞ | 80 | 20 | 2 | 7.324 | 7.642 | 7.483 | 4.25 | 2 |
| ∞ | 80 | 20 | 3 | 10.443 | 10.831 | 10.637 | 3.65 | 2 |
| ∞ | 80 | 20 | 4 | 13.209 | 13.649 | 13.429 | 3.28 | 2 |
| ∞ | 80 | 20 | 5 | 15.602 | 16.108 | 15.855 | 3.19 | 2 |
| ∞ | 80 | 30 | 1 | 5.176 | 5.431 | 5.304 | 4.81 | 2 |
| ∞ | 80 | 30 | 2 | 10.688 | 11.150 | 10.919 | 4.23 | 2 |
| ∞ | 80 | 30 | 3 | 15.400 | 15.932 | 15.666 | 3.40 | 2 |
| ∞ | 80 | 30 | 4 | 19.332 | 20.135 | 19.734 | 4.07 | 2 |
| ∞ | 80 | 30 | 5 | 22.904 | 23.766 | 23.335 | 3.69 | 2 |
| ∞ | 100 | 5 | 1 | 2.795 | 2.899 | 2.847 | 3.65 | 1 |
| ∞ | 100 | 5 | 2 | 5.172 | 5.294 | 5.233 | 2.33 | 2 |
| ∞ | 100 | 5 | 3 | 7.075 | 7.271 | 7.173 | 2.73 | 2 |
| ∞ | 100 | 5 | 4 | 8.675 | 8.955 | 8.815 | 3.18 | 2 |
| ∞ | 100 | 5 | 5 | 10.058 | 10.385 | 10.222 | 3.20 | 2 |
| ∞ | 100 | 10 | 1 | 4.431 | 4.566 | 4.499 | 3.00 | 1 |
| ∞ | 100 | 10 | 2 | 8.630 | 8.971 | 8.801 | 3.87 | 2 |
| ∞ | 100 | 10 | 3 | 12.062 | 12.546 | 12.304 | 3.93 | 2 |
| ∞ | 100 | 10 | 4 | 15.031 | 15.420 | 15.226 | 2.55 | 2 |
| ∞ | 100 | 10 | 5 | 17.605 | 18.062 | 17.834 | 2.56 | 2 |
| ∞ | 100 | 20 | 1 | 7.781 | 8.087 | 7.934 | 3.86 | 1 |
| ∞ | 100 | 20 | 2 | 15.500 | 15.996 | 15.748 | 3.15 | 2 |
| ∞ | 100 | 20 | 3 | 22.071 | 22.761 | 22.416 | 3.08 | 2 |
| ∞ | 100 | 20 | 4 | 27.697 | 28.530 | 28.114 | 2.96 | 2 |
| ∞ | 100 | 20 | 5 | 32.643 | 33.635 | 33.139 | 2.99 | 2 |
| ∞ | 100 | 30 | 1 | 10.931 | 11.475 | 11.203 | 4.86 | 2 |
| ∞ | 100 | 30 | 2 | 22.392 | 23.145 | 22.769 | 3.31 | 2 |
| ∞ | 100 | 30 | 3 | 32.016 | 33.159 | 32.588 | 3.51 | 2 |
| ∞ | 100 | 30 | 4 | 40.204 | 41.439 | 40.822 | 3.03 | 2 |
| ∞ | 100 | 30 | 5 | 47.565 | 48.929 | 48.247 | 2.83 | 2 |

between *GSI* and $\sigma_s/\sigma_{ci}$ is observed in Fig. 6. An increase of *GSI* results in a nonlinearly increase of $\sigma_s/\sigma_{ci}$. Such results can be referred to the exponential function used in the model of the HB failure criterion as expressed in Eqs. (2)–(4). The effect of $m_i$ is demonstrated in Fig. 7 that plots $m_i$ as the horizontal axis, where Fig. 7a, b, c, and d represent the cases of $GSI = 40$, 60, 80, and 100, respectively. All data in Fig. 7 are based on the constant value of $\sigma_{ci}/\gamma D = \infty$, and each line in the figure shows the *C/D* variation of 1–5. A linearly increasing relationship between $\sigma_s/\sigma_{ci}$ and $m_i$ is observed, which can be explained by the effect of the frictional strength of the intact rock mass expressed by $m_i$. Hence, an increase in $m_i$ results in a higher $\sigma_s/\sigma_{ci}$ of circular tunnels. Figure 8 shows the influence of $\sigma_{ci}/\gamma D$ on $\sigma_s/\sigma_{ci}$, where Fig. 8a, b, c, and d represent the cases of $C/D = 1$, 2, 4, and 5, respectively. Note that $m_i$ is equal to 20 for all curves in Fig. 8, and each line represents the *GSI* value varying from 40 to 100. It can be observed that the influence of $\sigma_{ci}/\gamma D$ on $\sigma_s/\sigma_{ci}$ is very small comparing with the other dimensionless parameters. In practice, the unit weight of rock masses ranging from 22 to 30 kN/m$^3$ has almost no effect on the failure surcharge over circular tunnels provided that $\sigma_{ci}/\gamma D$, $m_i$, *GSI*, and *C/D* remain constant.

The effect of *C/D* on the final adaptive meshes (5th iteration) representing the plastic shear zone of circular

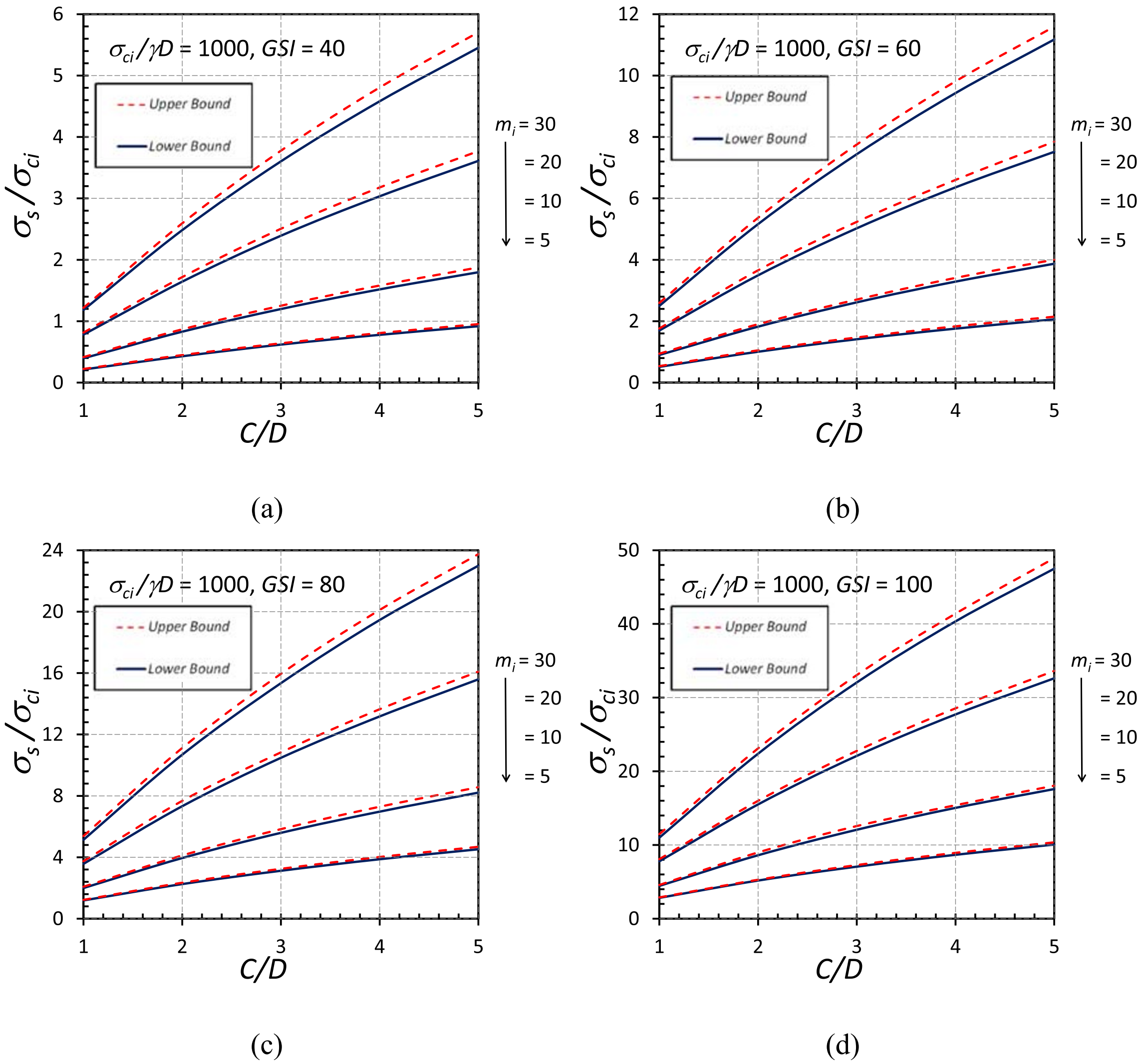


**Fig. 5** Influence of $C/D$ on $\sigma_s/\sigma_{ci}$ of circular tunnels with $\sigma_{ci}/\gamma D = 1000$: **a** $GSI = 40$, **b** $GSI = 60$, **c** $GSI = 80$, and **d** $GSI = 100$

tunnels in rock masses with $GSI = 60$, $m_i = 20$, and $\sigma_{ci}/\gamma D = 500$ is shown in Fig. 9a, b, c, and d corresponding to $C/D = 1$, $C/D = 2$, $C/D = 4$, and $C/D = 5$, respectively. In general, the failure zone resembles a circular shape that covers the tunnel and extends to the rock surface. An increase in $C/D$ results in the expansion of the circular failure zone around the tunnel as well as the expansion of that below its base. Closer inspections of all results of adaptive meshes reveal that there are two kinds of failure mechanism of circular tunnels in rock masses, namely (i) pattern 1: slip line originates from the tunnel wall (e.g., Fig. 9a) and (ii) pattern 2: slip line originates below the tunnel base (e.g., Fig. 9b–d). Note that the former corresponds to shallow tunnels with $C/H = 1$ while the latter corresponds to deeper ones with $C/H \geq 2$. These failure modes are also noted in the last column of Table 4.

Table 5 shows a comparison of the $\sigma_s/\sigma_{ci}$ solutions between circular and square tunnels in rock masses. Note that the former is the present study while the latter is based on the recent study of Ukritchon and Keawsawasvong (2019b) using only simulations of LB FELA. In general, the normalized failure pressure $\sigma_s/\sigma_{ci}$ of circular tunnels is relatively larger than that of square tunnels approximately by 20–70%. A higher stability of circular tunnels over square ones is mainly attributed an arching effect of stress distributions in circular tunnels. A similar finding was also reported in the previous FELA study of Yamamoto et al. (2011b) for tunnels in cohesive-frictional soils. In Table 5, a closer inspection reveals that a lower $C/D$ ratio tends to give a higher solution ratio between circular and square tunnels. In addition, $GSI$ and $m_i$ parameters also affect the difference of LB solutions between two tunnels. Large

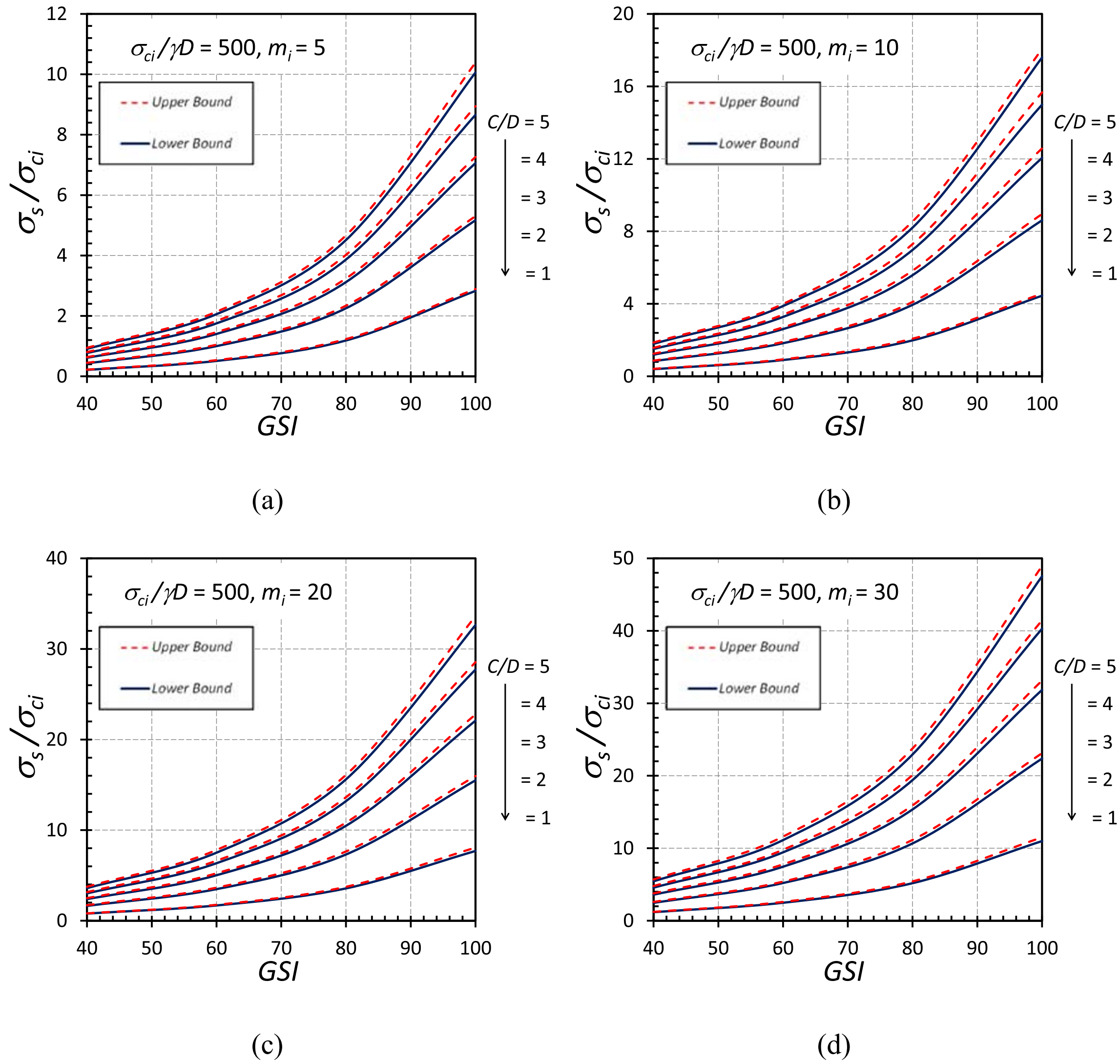


**Fig. 6** Influence of *GSI* on $\sigma_s/\sigma_{ci}$ of circular tunnels with $\sigma_{ci}/\gamma D = 500$: **a** $m_i = 5$, **b** $m_i = 10$, **c** $m_i = 20$, and **d** $m_i = 30$

differences of the solution ratios between circular and square tunnels can be observed for smaller *GSI* and higher $m_i$ values.

## Design equation for circular tunnels in rock masses

A curve fitting method is employed to develop an approximate expression for a collapse pressure over shallow unlined circular tunnels in rock masses. Based on Eq. (5) and the presented results in the preceding section, the normalized failure pressure $\sigma_s/\sigma_{ci}$ depends on a set of dimensionless parameters, namely cover-depth ratio *C/D*, Geological Strength Index *GSI*, Hoek-Brown $m_i$ parameter, and normalized uniaxial compressive strength $\sigma_{ci}/\gamma D$ of intact rocks. Since the differences between the computed UB and LB solutions are small within 5% of their average as shown in the previous section, their average values are taken as the approximate solution of the problem. The authors perform several trial-and-errors of a curve fitting technique on the average computed bound solutions of the problem in order to determine an appropriate mathematical expression. It is found that $\sigma_s/\sigma_{ci}$ can be well correlated with a quadratic function of *C/D*, a cubic function of *GSI*, a linear function of $m_i$, and a linear function of $\gamma D/\sigma_{ci}$, as shown below:

$$\frac{\sigma_s}{\sigma_{ci}} = A_1 + A_2\left(\frac{C}{D}\right) + A_3\left(\frac{C}{D}\right)^2 \tag{8a}$$

$$\frac{\sigma_s}{\sigma_{ci}} = B_1 + B_2(GSI) + B_3(GSI)^2 + B_4(GSI)^3 \tag{8b}$$

$$\frac{\sigma_s}{\sigma_{ci}} = E_1 + E_2(m_i) \tag{8c}$$

$$\frac{\sigma_s}{\sigma_{ci}} = G_1 + G_2\left(\frac{\gamma D}{\sigma_{ci}}\right) \tag{8d}$$

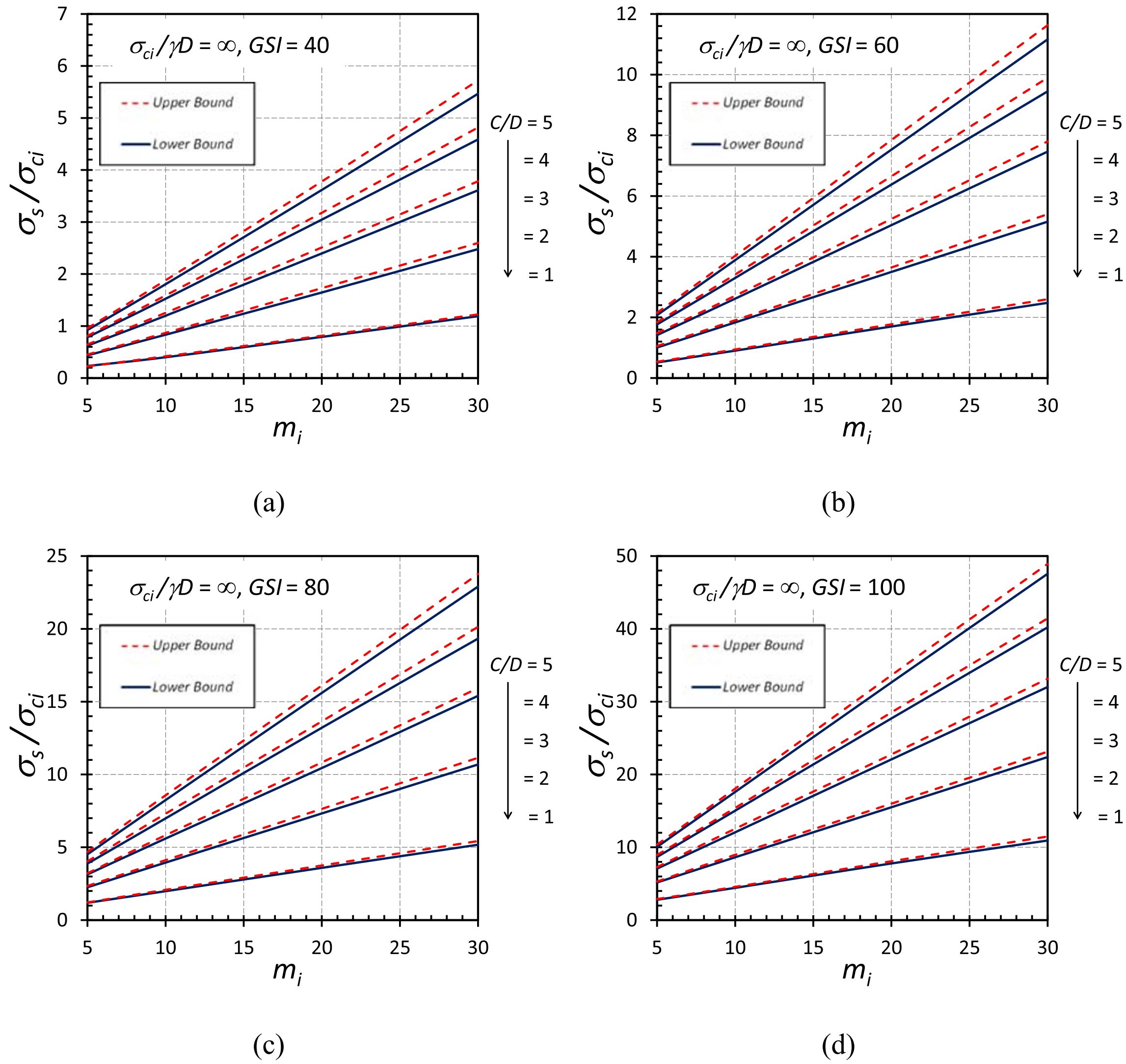


**Fig. 7** Influence of $m_i$ on $\sigma_s/\sigma_{ci}$ of circular tunnels with $\sigma_{ci}/\gamma D = \infty$: **a** $GSI = 40$, **b** $GSI = 60$, **c** $GSI = 80$, and **d** $GSI = 100$

where $A_i$, $B_i$, $E_i$, and $G_i$ are coefficients from curve fitting method if a set of remaining dimensionless parameters are selected.

Combining all mathematical functions in the preceding equations, a new design equation for the normalized failure surcharge $\sigma_s/\sigma_{ci}$ of shallow unlined circular tunnels in rock masses is proposed as:

$$\frac{\sigma_s}{\sigma_{ci}} = F_1 + F_2 m_i - F_3\left(\frac{\gamma D}{\sigma_{ci}}\right) \tag{9a}$$

$$F_1 = GSI\left[b_1 + b_2\frac{C}{D} + b_3\left(\frac{C}{D}\right)^2\right] + GSI^2\left[c_1 + c_2\frac{C}{D} + c_3\left(\frac{C}{D}\right)^2\right] \tag{9b}$$

$$F_2 = e_1 + e_2\frac{C}{D} + GSI\left[f_1 + f_2\frac{C}{D} + f_3\left(\frac{C}{D}\right)^2\right] + GSI^2\left[g_1 + g_2\frac{C}{D}\right] + GSI^3\left(d_2\frac{C}{D}\right) \tag{9c}$$

$$F_3 = a_1 + a_2\frac{C}{D} \tag{9d}$$

where $a_i$, $b_i$, $c_i$, $d_i$, $e_i$, $f_i$, and $g_i$ are constant coefficients.

The optimal value of the constant coefficients ($a_i$, $b_i$, $c_i$, $d_i$, $e_i$, $f_i$, and $g_i$) is solved by performing a least square method (Sauer, 2014; Walpole et al., 2002) that minimizes the sum of squares of the deviation (i.e., the error) in $\sigma_s/\sigma_{ci}$ between the computed average bound solutions and the approximate solutions (i.e., the predictions), as shown below.

$$\text{Minimize}\left(\text{error}^2\right) = \text{Minimize}\left(\sum_{i=1}^{n}\left(y_i - f_i\right)^2\right) \tag{10}$$

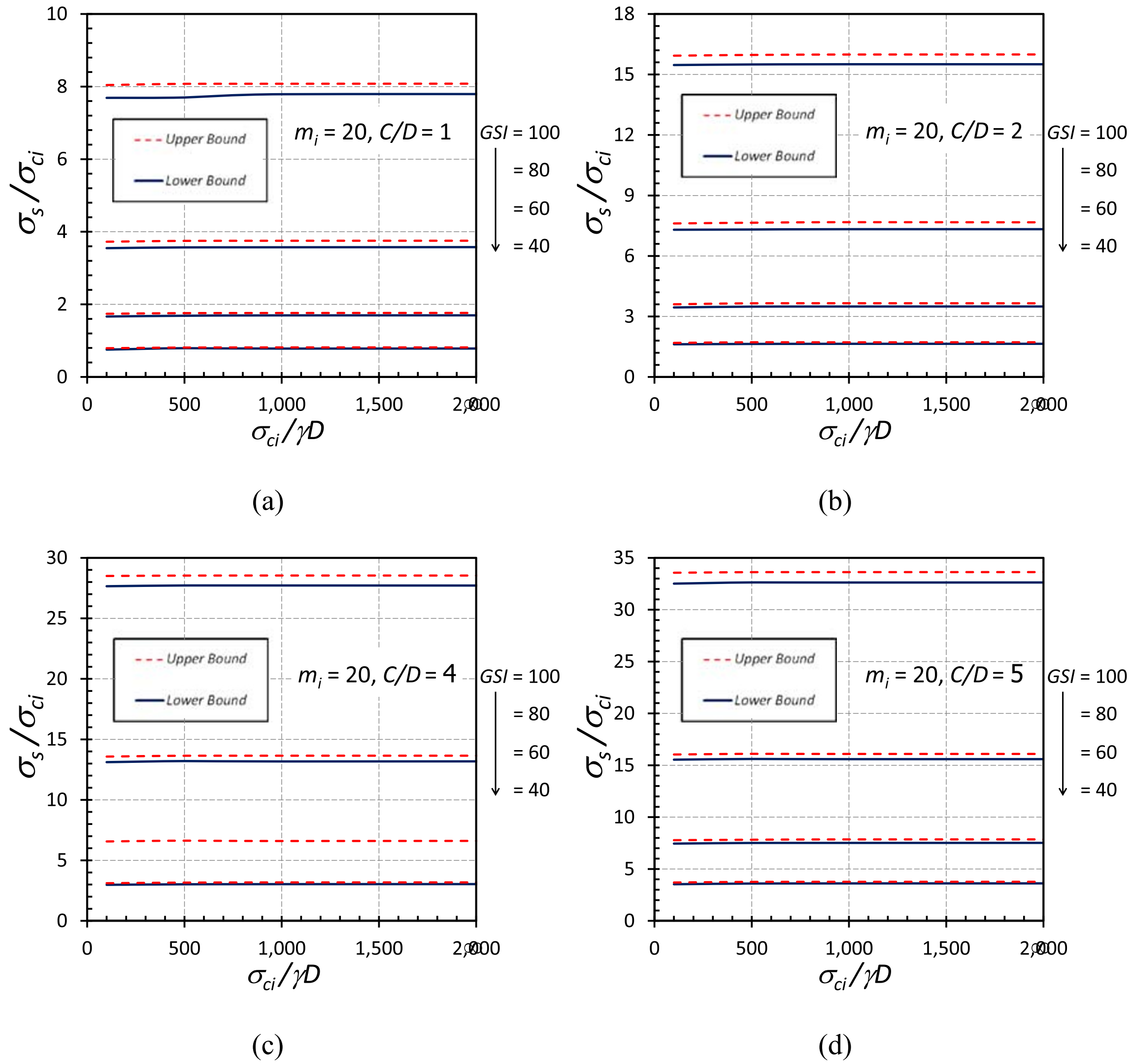


**Fig. 8** Influence of $\sigma_{ci}/\gamma D$ on $\sigma_s/\sigma_{ci}$ of circular tunnels with $m_i = 20$: **a** $C/D = 1$, **b** $C/D = 2$, **c** $C/D = 4$, and **d** $C/D = 5$

where $y_i$ is the average computed bound solution, $f_i$ is the approximate solution of $\sigma_s/\sigma_{ci}$ from Eq. (9a), and $n$ is the number of data.

The accuracy of the proposed new design equation can be verified using the coefficient of determination, $R^2$ (Sauer, 2014; Walpole et al., 2002) as:

$$R^2 = 1 - \frac{SS_{\text{res}}}{SS_{\text{tot}}} \tag{11}$$

where $SS_{\text{tot}} = \sum_{i=1}^{n} (y_i - \bar{y})^2$, $SS_{\text{res}} = \sum_{i=1}^{n} (y_i - f_i)^2$, and $\bar{y} = \frac{1}{n}\sum_{i=1}^{n} y_i$.

Employing the least square method to the proposed expression in Eq. (9a) and the total number of average bound solutions of 320, the optimal value of the constant coefficients ($a_i$, $b_i$, $c_i$, $d_i$, $e_i$, $f_i$, and $g_i$) is found, as summarized in Table 6. Figure 10 illustrates the comparison of $\sigma_s/\sigma_{ci}$ between the predictions of the proposed new design equation and the average bound solutions. It can be observed that good agreement between them is well observed, where the coefficient of determination ($R^2$) was 99.98%. Thus, the proposed new design equation in Eq. (9a) is reasonably accurate in predicting the failure surcharge of shallow unlined circular tunnels in rock masses.

The proposed design equation in Eq. (9a) can be rewritten as another mathematical form that reflects the uniaxial compressive strength of intact rocks and their unit weight as:

$$\sigma_s = N_c\sigma_{ci} - N_\gamma \gamma D \tag{12a}$$

$$N_c = F_1 + F_2 m_i \tag{12b}$$

$$N_\gamma = F_3 \tag{12c}$$

It should be noted that the $N_c$ factor represents the effect of the uniaxial compressive strength of intact rock $\sigma_{ci}$, which is a function of $C/D$, $GSI$, and $m_i$, as shown in Fig. 11. The $N_\gamma$

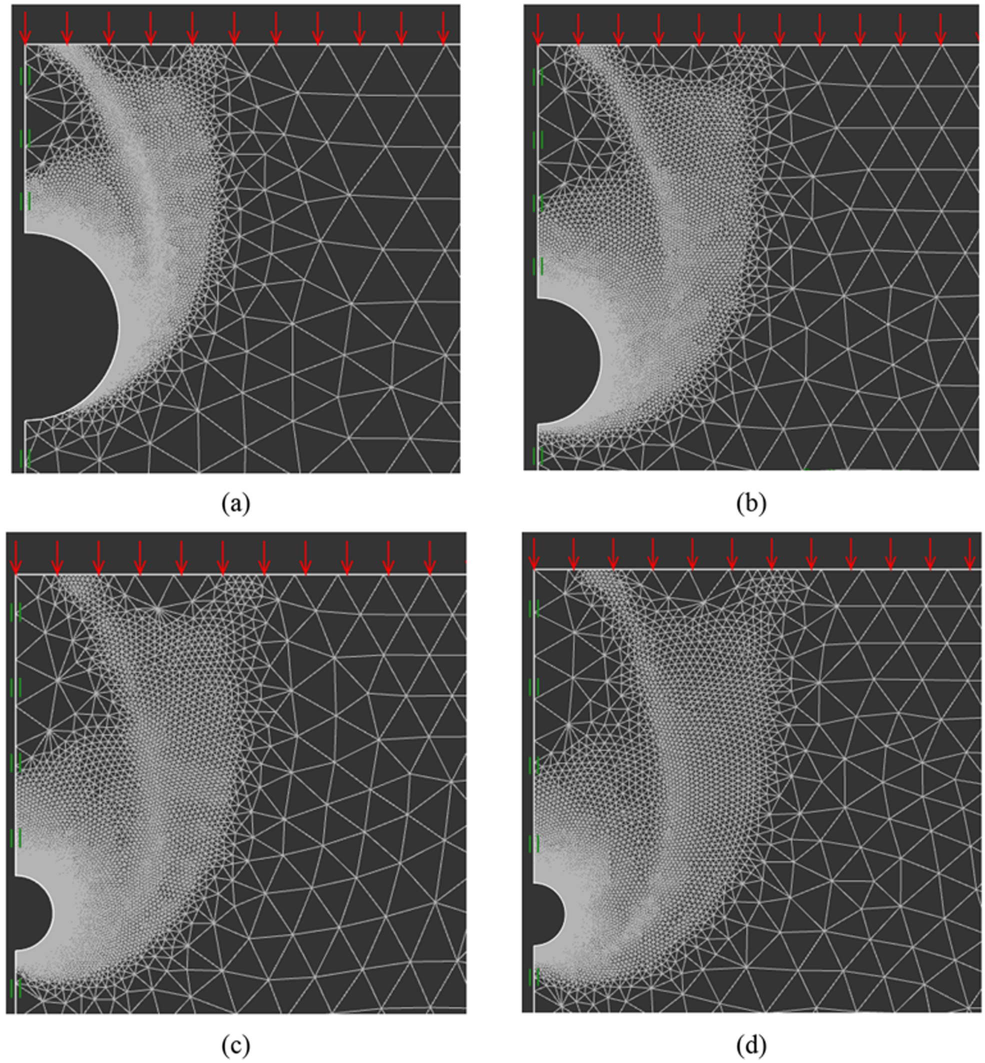

**Fig. 9** Final adaptive meshes for the cases of $GSI = 60$, $m_i = 20$, $\sigma_{ci}/\gamma D = 500$: **a** $C/D = 1$, **b** $C/D = 2$, **c** $C/D = 4$, and **d** $C/D = 5$

factor represents the effect of rock unit weight $\gamma$, which depends on only $C/D$, as shown in Fig. 12. It can be observed that the predictions of the failure surcharge over shallow unlined circular tunnels in rock masses can be conveniently performed using the proposed design equation in Eq. (12a).

Even though good agreement between the proposed design equation and the computed numerical solutions is observed, the proposed equations have some limitations that are associated with assumptions of the numerical modelling. First, the applications of the proposed equations should be strictly applied within the selected ranges of dimensionless parameters, namely $C/D = 1$–5, $GSI = 40$–100, $m_i = 5$–30, and $\sigma_{ci}/\gamma D =$ 100–$\infty$ since they are based on a curve fitting technique that seems to work well only for interpolations. Second, rock masses should be homogenous and should not have any distinct bedding plane since their homogenous and isotropic failure behaviors are assumed in the numerical modeling. Last, the results cannot be applied to circular tunnels that are affected by damage and stress relaxation since the $DF$ parameter accounting for those effects is neglected in the present study (i.e., $DF = 0$).

## Conclusions

In this paper, the stability of shallow unlined circular tunnels in rock masses is investigated by employing the upper and lower bound finite element limit analysis. For the first time, the present study performs a comprehensively numerical investigations of the full set of dimensionless parameters of the problem including cover-depth ratio $C/D$ of 1–5, Geological Strength Index $GSI$ of 40–100, Hoek-Brown $m_i$ parameter of 5–30, and the normalized uniaxial compressive strength $\sigma_{ci}/\gamma D$ of 100–$\infty$. Powerful and efficient computational finite element limit analysis with adaptive meshing procedure is employed in order to compute accurate bound solutions of the problem. In all cases, the present study can accurately bracket the true solution of the problem by upper and lower

**Table 5** Comparison of the solutions between circular and square tunnels

| $\sigma_{ci}/\gamma H$ | $GSI$ | $m_i$ | $C/H$ | Circular tunnels | | Square tunnels | $(LB)_{cr}/(LB)_{sq}$ |
|---|---|---|---|---|---|---|---|
| | | | | Present study | | Ukritchon and Keawsawasvong (2019b) | |
| | | | | $\sigma_s/\sigma_{ci}$ $(LB)_{cr}$ | $\sigma_s/\sigma_{ci}$ $(UB)_{cr}$ | $\sigma_s/\sigma_{ci}$ $(LB)_{sq}$ | |
| 100 | 60 | 5 | 1 | 0.496 | 0.514 | 0.336 | 1.476 |
| 100 | 60 | 5 | 2 | 0.973 | 1.000 | 0.714 | 1.364 |
| 100 | 60 | 5 | 3 | 1.369 | 1.426 | 1.062 | 1.289 |
| 100 | 60 | 5 | 4 | 1.706 | 1.776 | 1.373 | 1.243 |
| 100 | 60 | 5 | 5 | 2.001 | 2.080 | 1.641 | 1.219 |
| 100 | 60 | 30 | 1 | 2.472 | 2.577 | 1.463 | 1.689 |
| 100 | 60 | 30 | 2 | 5.114 | 5.364 | 3.556 | 1.438 |
| 100 | 60 | 30 | 3 | 7.402 | 7.762 | 5.291 | 1.399 |
| 100 | 60 | 30 | 4 | 9.380 | 9.739 | 6.631 | 1.414 |
| 100 | 60 | 30 | 5 | 11.240 | 11.540 | 7.549 | 1.489 |
| 100 | 100 | 5 | 1 | 2.788 | 2.875 | 2.038 | 1.368 |
| 100 | 100 | 5 | 2 | 5.140 | 5.283 | 3.913 | 1.314 |
| 100 | 100 | 5 | 3 | 7.032 | 7.246 | 5.574 | 1.262 |
| 100 | 100 | 5 | 4 | 8.610 | 8.899 | 7.082 | 1.216 |
| 100 | 100 | 5 | 5 | 9.997 | 10.314 | 8.328 | 1.200 |
| 100 | 100 | 30 | 1 | 10.966 | 11.491 | 6.909 | 1.587 |
| 100 | 100 | 30 | 2 | 22.316 | 23.117 | 16.059 | 1.390 |
| 100 | 100 | 30 | 3 | 31.988 | 33.027 | 24.288 | 1.317 |
| 100 | 100 | 30 | 4 | 40.265 | 41.361 | 31.355 | 1.284 |
| 100 | 100 | 30 | 5 | 47.457 | 48.833 | 37.420 | 1.268 |

bound solutions within 5% with respect to their average values. It is found that the normalized failure surcharge $\sigma_s/\sigma_{ci}$ over shallow unlined circular tunnel has a nonlinear relationship between $C/D$ and $GSI$, and a linear relationship between $m_i$ and $\gamma D/\sigma_{ci}$. The predicted failure mechanism of shallow unlined circular tunnels resembles a circular zone that spreads laterally and deeply into rock masses as $C/D$ increases. When $C/D$ is equal to or greater than 2, it is observed that the circular failure zone develops below the invert of tunnels. A new design equation of the failure surcharge of the problem is proposed using a least square method of the computed average bound solutions. The performance of the proposed new design equation is accurately achieved and is verified by good agreement between the predictions and computed average bound solutions, where the coefficient of determination is very high of 99.98%. The proposed design equation provides a new accurate tool for practical stability analyses of shallow unlined circular tunnels in rock masses obeying the Hoek-Brown failure criterion. In practice, the failure surcharge can be conveniently and accurately predicted by using the proposed new tunnel stability factors $N_c$ and $N_\gamma$. The influences of the cover-depth ratio of tunnels, the uniaxial compressive strength of intact rocks, Geological Strength Index, and the $m_i$ Hoek-Brown parameter on the failure surcharge of the problem are reflected in the new tunnel stability factors. The future works relating to this paper can be performed by

**Table 6** Optimal value of the constants for the new design equation of $\sigma_s/\sigma_{ci}$ for unlined circular tunnels in rock masses using nonlinear regression

| $a_1$ | $a_2$ | $b_1$ | $b_2$ | $b_3$ | $c_1$ | $c_2$ | $c_3$ | $d_1$ |
|---|---|---|---|---|---|---|---|---|
| 0.6649 | 1.1415 | 0.02254 | $-0.03034$ | $0.4432 \times 10^{-2}$ | $-0.2317 \times 10^{-3}$ | $0.4186 \times 10^{-3}$ | $-0.5789 \times 10^{-4}$ | $1.056 \times 10^{-6}$ |

| $a_1$ | $e_1$ | $e_2$ | $f_1$ | $f_2$ | $f_3$ | $g_1$ | $g_2$ |
|---|---|---|---|---|---|---|---|
| 0.6649 | 0.08065 | $-0.1368$ | $-0.3936 \times 10^{-2}$ | $0.9536 \times 10^{-2}$ | $-0.1555 \times 10^{-3}$ | $0.2903 \times 10^{-4}$ | $-0.1483 \times 10^{-3}$ |

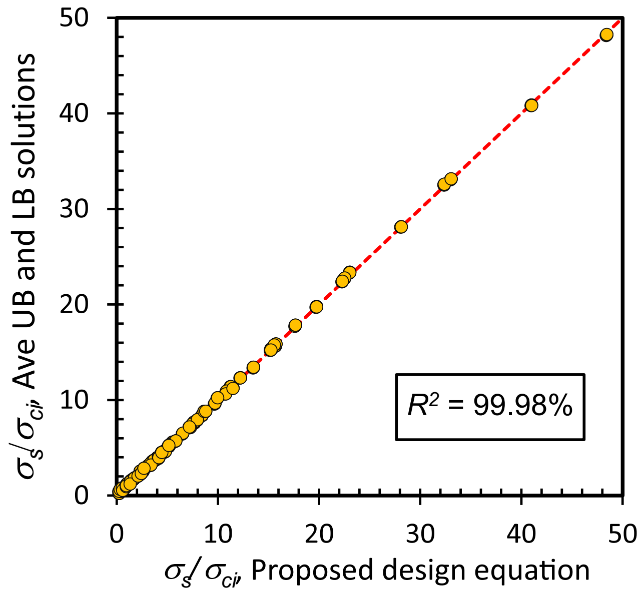


**Fig. 10** Comparison of the normalized failure surcharge $\sigma_s/\sigma_{ci}$ between the proposed design equation and the computed average bound solutions

studying the effect of the disturbance factor *DF* or the effect of water seepage through circular tunnels. In addition, the

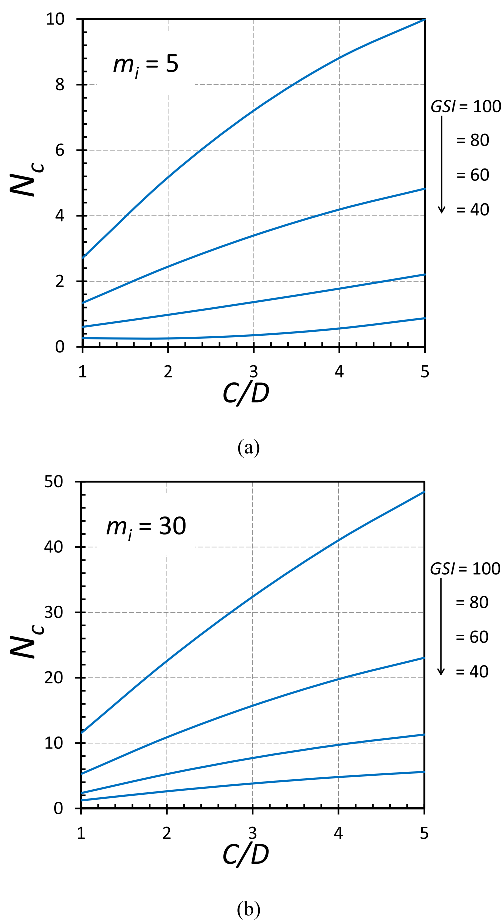


**Fig. 11** Proposed stability factors $N_c$ of shallow unlined circular tunnels in Hoek-Brown rock masses: **a** $m_i = 5$, **b** $m_i = 30$

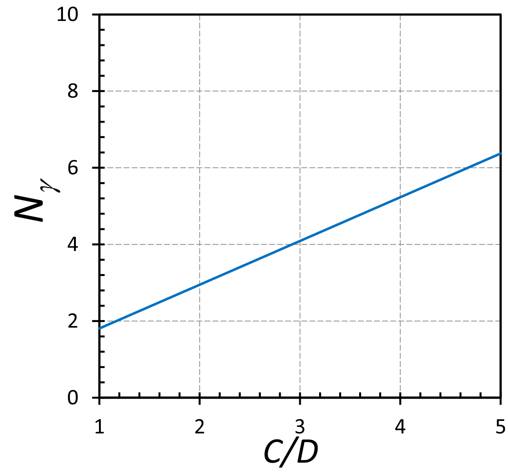


**Fig. 12** Proposed stability factors $N_\gamma$ of shallow unlined circular tunnels in Hoek-Brown rock masses

stability of the present problem can be studied in three-dimensional coordinate system, which is more realistic in practice.

## References


Akin M (2013) Slope stability problems and back analysis in heavily jointed rock mass: a case study from Manisa, Turkey. Rock Mech Rock Eng 46:359–371

Assadi A, Sloan SW (1991) Undrained stability of shallow square tunnel. J Geotech Eng 117(8):1152–1173

Augarde CE, Lyamin AV, Sloan SW (2003) Stability of an undrained plane strain heading revisited. Comput Geotech 30(5):419–430

Belghali M, Saada Z, Garnier D, Maghous S (2017) Pseudo-static stability analysis of rock slopes reinforced by passive bolts using the generalized Hoek-Brown criterion. J Rock Mech Geotech Eng 9: 659–670

Butterfield R (1999) Dimensional analysis for geotechnical engineering. Géotechnique 49(2):357–366

Carranza-Torres C (2004) Elasto-plastic solution of tunnel problems using the generalized form of the Hoek-Brown failure criterion. Int J Rock Mech Min Sci 41:480–481

Carranza-Torres C, Fairhurst C (1999) The elasto-plastic response of underground excavations in rock masses that satisfy the Hoek-Brown failure criterion. Int J Rock Mech Min Sci 36:777–809

Chakraborty M, Kumar J (2015) Bearing capacity of circular footings over rock mass by using axisymmetric quasi lower bound finite element limit analysis. Comput Geotech 70:138–149

Chambon P, Corté JF (1994) Shallow tunnels in cohesionless soil: stability of tunnel face. J Geotech Eng 120:1148–1165

Chen WF, Liu XL (1990) Limit analysis in soil mechanics. Elsevier, Amsterdam

Ciria H, Peraire J, Bonet J (2008) Mesh adaptive computation of upper and lower bounds in limit analysis. Int J Numer Methods Eng 75: 899–944

Clausen J (2013) Bearing capacity of circular footings on a Hoek-Brown material. Int J Rock Mech Min Sci 57:34–41

Davis EH, Gunn MJ, Mair RJ, Seneviratine HN (1980) The stability of shallow tunnels and underground openings in cohesive material. Geotechnique 30:397–416

Deng D, Li L, Wang J, Zhao L (2016) Limit equilibrium method for rock slope stability analysis by using the Generalized Hoek–Brown criterion. Int J Rock Mech Min Sci 89:176–184

Drucker DC, Prager W, Greenberg HJ (1952) Extended limit design theorems for continuous media. Q Appl Math 9:381–389

Fraldi M, Guarracino F (2009) Limit analysis of collapse mechanisms in cavities and tunnels according to the Hoek–Brown failure criterion. Int J Rock Mech Min Sci 46:665–673

Hoek E (2004) A brief history of the development of the Hoek–Brown failure criterion; Available at: http://www.rocscience.com

Hoek E (2007) Practical rock engineering. Available at: http://www.rocscience.com

Hoek E, Brown ET (1980) Empirical strength criterion for rock masses. J Geotech Eng Div 106(9):1013–1035

Hoek E, Carranza-Torres C, Corkum B (2002) Hoek–Brown failure criterion—2002 edition. In: Proceedings of the North American rock mechanics society meeting in Toronto

Keawsawasvong S, Ukritchon B (2016a) Ultimate lateral capacity of two dimensional plane strain rectangular pile in clay. Geomech Eng 11(2):235–251

Keawsawasvong S, Ukritchon B (2016b) Finite element limit analysis of pullout capacity of planar caissons in clay. Comput Geotech 75:12–17

Keawsawasvong S, Ukritchon B (2017a) Undrained limiting pressure behind soil gaps in contiguous pile walls. Comput Geotech 83: 152–158

Keawsawasvong S, Ukritchon B (2017b) Undrained stability of an active planar trapdoor in non-homogeneous clays with a linear increase of strength with depth. Comput Geotech 81:284–293

Keawsawasvong S, Ukritchon B (2017c) Stability of unsupported conical excavations in non-homogeneous clays. Comput Geotech 81:125–136

Keawsawasvong S, Ukritchon B (2017d) Finite element analysis of undrained stability of cantilever flood walls. Int J Geotech Eng 11(4): 355–367

Keawsawasvong S, Ukritchon B (2017e) Undrained lateral capacity of I-shaped concrete piles. Songklanakarin J Sci Technol 39(6):751–758

Keawsawasvong S, Ukritchon B (2019a) Undrained stability of a spherical cavity in cohesive soils using finite element limit analysis. J Rock Mech Geotech Eng 11(6):1274–1285

Keawsawasvong S, Ukritchon B (2019b) Undrained basal stability of braced circular excavations in non-homogeneous clays with linear increase of strength with depth. Comput Geotech 115:103180

Keshavarz A, Kumar J (2018) Bearing capacity of foundations on rock mass using the method of characteristics. Int J Numer Anal Methods Geomech 42(3):542–557

Keshavarz A, Fazeli A, Sadeghi S (2016) Seismic bearing capacity of strip footings on rock masses using the Hoek-Brown failure criterion. J Rock Mech Geotech Eng 8:170–177

Kimura T, Mair RJ (1981) Centrifugal testing of model tunnels in soft clay. In: Proceedings of 10th International Conference on Soil Mechanics and Foundation Engineering, Stockholm, 15–19 June 1981. Rotterdam: Balkema, p 319–22

Kirsch A (2010) Experimental investigation of the face stability of shallow tunnels in sand. Acta Geotech 5:43–62

Krabbenhoft K, Lyamin A, Krabbenhoft J (2015) Optum computational engineering (OptumG2); Available at: www.optumce.com

Kumar J, Mohapatra D (2017) Lower-bound finite elements limit analysis for Hoek-Brown materials using semidefinite programming. J Eng Mech 143(9):04017077

Li AJ, Merifield RS, Lyamin AY (2008) Stability charts for rock slopes based on the Hoek–Brown failure criterion. Int J Rock Mech Min Sci 45:689–700

Li A, Merifield R, Lyamin A (2011) Effect of rock mass disturbance on the stability of rock slopes using the Hoek-Brown failure criterion. Comput Geotech 38(4):546–558

Merifield RS, Lyamin AV, Sloan W (2006) Limit analysis solutions for the bearing capacity of rock masses using the generalized Hoek-Brown yield criterion. Int J Rock Mech Min Sci 43:920–937

Sauer T (2014) Numerical analysis. London, Pearson Education Limited

Senent S, Mollon G, Jimenez R (2013) Tunnel face stability in heavily fractured rock masses that follow the Hoek–Brown failure criterion. Int J Rock Mech Min Sci 60:440–451

Serrano A, Olalla C (1998a) Ultimate bearing capacity of an anisotropic discontinuous rock mass, part I: basic modes of failure. Int J Rock Mech Min Sci 35(3):301–324

Serrano A, Olalla C (1998b) Ultimate bearing capacity of an anisotropic discontinuous rock mass, part II: determination procedure. Int J Rock Mech Min Sci 35(3):325–348

Serrano A, Olalla C, Galindo RA (2014) Ultimate bearing capacity at the tip of a pile in rock based on the modified Hoek–Brown criterion. Int J Rock Mech Min Sci 71:83–90

Serrano A, Olalla C, Galindo RA (2015) Shaft resistance of a pile in rock based on the modified Hoek–Brown criterion. Int J Rock Mech Min Sci 76:138–145

Serrano A, Olalla C, Galindo RA (2016) Ultimate bearing capacity of an anisotropic discontinuous rock mass based on the modified Hoek–Brown criterion. Int J Rock Mech Min Sci 83:24–40

Shen JY, Karakus M, Xu CS (2013) Chart-based slope stability assessment using the Generalized Hoek–Brown criterion. Int J Rock Mech Min Sci 64:210–219

Sloan SW (2013) Geotechnical stability analysis. Géotechnique 63(7): 531–572

Sloan SW, Assadi A (1991) Undrained stability of a square tunnel in a soil whose strength increases linearly with depth. Comput Geotech 12(4):321–346

Sloan SW, Assadi A (1994) Undrained stability of a plane strain heading. Can Geotech J 31:443–450

Ukritchon B, Keawsawasvong S (2016) Undrained pullout capacity of cylindrical suction caissons by finite element limit analysis. Comput Geotech 80:301–311

Ukritchon B, Keawsawasvong S (2017a) Design equations for undrained stability of opening in underground walls. Tunn Undergr Space Technol 70:214–220

Ukritchon B, Keawsawasvong S (2017b) Error in Ito and Matsui's limit equilibrium solution of lateral force on a row of stabilizing piles. J Geotech Geoenviron 143(9):02817004

Ukritchon B, Keawsawasvong S (2017c) Unsafe error in conventional shape factor for shallow circular foundations in normally consolidated clays. J Geotech Geoenviron 143(6):02817001

Ukritchon B, Keawsawasvong S (2018a) Lower bound limit analysis of an anisotropic undrained strength criterion using second-order cone programming. Int J Numer Anal Methods Geomech 42(8):1016–1033

Ukritchon B, Keawsawasvong S (2018b) Three-dimensional lower bound finite element limit analysis of Hoek-Brown material using semidefinite programming. Comput Geotech 104:248–270

Ukritchon B, Keawsawasvong S (2018c) Undrained lateral capacity of rectangular piles under a general loading direction and full flow mechanism. KSCE J Civ Eng 22(7):2256–2265

Ukritchon B, Keawsawasvong S (2018d) A new design equation for drained stability of conical slopes in cohesive-frictional soils. J Rock Mech Geotech Eng 10:358–366

Ukritchon B, Keawsawasvong S (2019a) Stability of retained soils behind underground walls with an opening using lower bound limit analysis and second-order cone programming. Geotech Geol Eng 37(3): 1609–1625

Ukritchon B, Keawsawasvong S (2019b) Stability of unlined square tunnels in Hoek-Brown rock masses based on lower bound analysis. Comput Geotech 105:249–264

Ukritchon B, Keawsawasvong S (2019c) Lower bound stability analysis of plane strain headings in Hoek-Brown rock masses. Tunn Undergr Space Technol 84:99–112

Ukritchon B, Keawsawasvong S (2019d) Three-dimensional lower bound finite element limit analysis of an anisotropic undrained strength criterion using second-order cone programming. Comput Geotech 106:327–344

Ukritchon B, Keawsawasvong S (2019e) Lower bound solutions for undrained face stability of plane strain tunnel heading in anisotropic and non-homogeneous clays. Comput Geotech 112:204–217

Ukritchon B, Keawsawasvong S (2019f) Design equations of uplift capacity of circular piles in sands. Appl Ocean Res 90:101844

Ukritchon B, Yoang S, Keawsawasvong S (2018) Bearing capacity of shallow foundations in clay with linear increase in strength and adhesion factor. Mar Georesour Geotechnol 36(4):438–451

Ukritchon B, Yoang S, Keawsawasvong S (2019) Three-dimensional stability analysis of the collapse pressure on flexible pavements over rectangular trapdoors. Transp Geotech 21:100277

Ukritchon B, Yoang S, Keawsawasvong S (2020) Undrained stability of unsupported rectangular excavations in non-homogeneous clays. Comput Geotech 117:103281

Walpole RE, Myers RH, Myers SL, Ye K (2002) Probability & statistics for engineering and scientists 7th ed, Prentice Hall, New Jersey, USA

Wilson DW, Abbo AJ, Sloan SW, Lyamin AV (2011) Undrained stability of a circular tunnel where the shear strength increases linearly with depth. Can Geotech J 48(9):1328–1342

Wilson DW, Abbo AJ, Sloan SW, Lyamin AV (2013) Undrained stability of a square tunnel where the shear strength increases linearly with depth. Comput Geotech 49:314–325

Xiao Y, Zhao M, Zhao H, Zhang R (2018) Finite element limit analysis of the bearing capacity of strip footing on a rock mass with voids. Int J Geomech 18(9):04018108

Yamamoto K, Lyamin AV, Wilson DW, Sloan SW, Abbo AJ (2011a) Stability of a circular tunnel in cohesive-frictional soil subjected to surcharge loading. Comput Geotech 38(4):504–514

Yamamoto K, Lyamin AV, Wilson DW, Sloan SW, Abbo AJ (2011b) Stability of a single tunnel in cohesive–frictional soil subjected to surcharge loading. Can Geotech J 48(12):1841–1854

Yang XL, Huang F (2011) Collapse mechanism of shallow tunnel based on nonlinear Hoek-Brown failure criterion. Tunn Undergr Space Technol 26(6):686–691

Yang XL, Huang F (2013) Three-dimensional failure mechanism of a rectangular cavity in a Hoek–Brown rock medium. Int J Rock Mech Min Sci 61:189–195

Yang XL, Li L, Yin JH (2004) Stability analysis of rock slopes with a modified Hoek–Brown failure criterion. Int J Numer Anal Methods Geomech 28:181–190

Yang F, Zhang J, Zhao L, Yang J (2016) Upper-bound finite element analysis of stability of tunnel face subjected to surcharge loading in cohesive-frictional soil. KSCE J Civ Eng 20(6):2270–2279